NASA TECHNICAL MEMORANDUM

NASA TM X-62,123

NASA TM X-62,123

NAVIGATION FOR SPACE SHUTTLE APPROACH AND LANDING USING AN INERTIAL NAVIGATION SYSTEM AUGMENTED BY DATA FROM A PRECISION RANGING SYSTEM OR A MICROWAVE SCAN BEAM LANDING GUIDANCE SYSTEM

L. A. McGee, G. L. Smith, D. M. Hegarty, R. B. Merrick, T. M. Carson, and S. F. Schmidt

Ames Research Center
Moffett Field, Ca. 94035

and

Analytical Mechanics Associates
Mountain View, Ca. 94040

December 1970

NAVIGATION FOR SPACE SHUTTLE APPROACH AND LANDING USING AN INERTIAL NAVIGATION SYSTEM AUGMENTED BY DATA FROM A PRECISION RANGING SYSTEM OR A MICROWAVE SCAN BEAM LANDING GUIDANCE SYSTEM

by

L.A. McGee, G.L. Smith, D.M. Hegarty
R.B. Merrick, T.M. Carson
Ames Research Center
and
S.F. Schmidt
Analytical Mechanics Associates

SUMMARY

A preliminary study has been made of the navigation performance which might be achieved for the high cross-range space shuttle orbiter during final approach and landing by using an optimally augmented Inertial Navigation System.

Computed navigation accuracies are presented for an on-board inertial navigation system augmented (by means of an optimal filter algorithm) with data from two different ground navigation aids; a precision ranging system and a microwave scanning beam landing guidance system. These results show that augmentation with either type of ground navigation aid is capable of providing a navigation performance at touchdown which should be adequate for the space shuttle. In addition, adequate navigation performance for space shuttle landing is obtainable from the precision ranging system even with a complete dropout of precision range measurements as much as 100 seconds before touchdown.

INTRODUCTION

Elimination of the air-breathing engines on the space shuttle orbiter and the associated fuel could provide substantial increases in the orbiter payload (Reference 1). These and other considerations provide considerable motivation for examining the feasibility of the unpowered flight mode. To attain a high probability of a successful landing in the unpowered mode requires a precision navigation system, particularly during approach and landing.

Recent investigations in estimation techniques have indicated that an inertial navigation system (INS), augmented by external information from

ground-based navigation aids, has the possibility of providing the navigation precision required.

This study presents preliminary results obtained from a full-scale digital simulation of a sophisticated on-board navigation system called RAINPAL (Recursive Aided Inertial Navigation for Precision Approach and Landing) which is under development at the NASA Ames Research Center. The RAINPAL system consists of a LTN-51 inertial navigation system, ground-based navigation aids, and a filter algorithm programmed in an on-board digital computer for optimally combining the data from various external data sources. The primary objective of the RAINPAL study is proof-of-concept by actual flight test.

The results from this program will provide information applicable to the space shuttle, as well as conventional jet transports and STOL vehicles. Two of the ground navigation aids considered in this preliminary study are:

(1) A precision ranging system (PRS) designed to provide precision range measurements from multiple, accurately known ground transponder locations. In this report, the PRS is modeled after a system Ames Research Center has operated on board a CV-340 aircraft for several years (Reference 2) and represents the performance which is presently believed to be available from the system.

(2) A microwave scan beam (MSB) landing guidance system concept which is being considered as the future standard for commercial aviation. The MSB is modeled after the Advanced Integrated Landing System (AILS) test results which were obtained at the National Aviation Facilities Experimental Center (NAFEC).

NOMENCLATURE

X, Y, Z	Cartesian coordinates of SSV position
$\dot{X}, \dot{Y}, \dot{Z}$	Cartesian coordinates of SSV velocity

SYSTEM DESCRIPTION

RAINPAL Formulation

Only the most cursory description of the mechanization will be presented here. Figure 1 presents a conceptual block diagram of the mechanization as it is presently planned in the Ames RAINPAL study. If the RAINPAL concept is used for the SSV, the mechanization need not have precisely the RAINPAL configuration but its performance and method of operation would be essentially the same. The figure shows specific forces acting on the vehicle, such as control inputs, winds, etc., which are measured by three accelerometers in the inertial measurement unit (IMU) which has errors as indicated. These

accelerations are quantized and summed in the interface to produce Δv words (changes in velocity) which are transformed into runway coordinates. In the navigation equations, after the effect of the computed gravity is removed and coriolis corrections made, a second integration is performed to obtain position. The output of the navigation equations is an estimated eleven-state vector $\hat{x}$. As shown in Figure 1, this eleven-state vector is corrected by estimated changes in the state vector, $\Delta\hat{x}$, produced by the Kalman filter to give a corrected estimate $\hat{x}'$. The Kalman filter produces these estimates by sampling external measurements, y, as shown. It should be noted that the system is capable of pure 3-axis inertial operation when the vertical (Z) channel is stabilized by a barometric altimeter or some other source of data containing altitude information.

The errors included in the estimated state vector are the platform tilt errors, the vertical accelerometer bias, and the barometric altimeter bias as shown in Figure 1. Preliminary analyses for RAINPAL have indicated these to be the most important error sources. These analyses have been verified by other simulation results.

Errors which are not elements of the estimated state vector include, for example, gyro and accelerometer misalignments, gyro drift rates, and external measurement biases. Although not estimated, realistic values of all error sources considered significant were included in the simulation program. A standard technique to reduce the effect of these errors which are not estimates is used; pseudo-random forcing functions are added in the Kalman filter to increase the filter's weighting of the more recent external measurements.

COMPONENT ACCURACIES

Inertial Measurement Unit (IMU). The errors in the IMU portion of the INS were provided by the NASA Manned Spacecraft Center and are presented in Table I. The Table shows the 1-sigma value to be expected with software calibration in the center column and the 3-sigma errors to be expected from the basic instrument.

Sensor Error Models. The error models used in the study for the PRS, the MSB and the barometric altimeter are given in Table II. The error for the PRS model is based primarily on Ames operational experience with this system. One important quantity not shown in the Table is the minimum useable range to a transponder. Operational experience shows this to be of the order of 50 feet. The error model for the MSB is based on reports of actual flight tests of the AILS microwave scanning beam system at NAFEC and reported by the C.S. Draper Laboratory, M.I.T. in Reference 3 except that one milliradian of bias was added to both the azimuth and elevation measurements to account for mounting and alignment errors. The barometric altimeter error model was based on preliminary information regarding the error characteristics of a class of barometric altimeters which use a capacitive element to sense barometric pressure. The particular simplified model chosen in this case was for a low-altitude range device which was to be used only for landing approach studies with the RAINPAL system. The effects of static port errors due to

vehicle angle of attack, velocity, etc., were not considered. In addition, the effect of non-standard atmosphere was assumed to be included in the bias figure.

STUDY CONDITIONS

Trajectory and Ground Navigation Aids. The trajectory used in this study is indicated in Figure 2. It is a straight-in approach, flare, and touchdown path with velocity and flight path angle characteristic of the North American Rockwell delta-wing orbiter. The flight time is 244 seconds. The transponder geometry for the PRS and the MSB azimuth and elevation scanners and DME which is part of the azimuth scanner is also shown in Figure 2.

The placement of the transponders relative to the origin of the runway coordinate system is dependent upon the expected vehicle trajectory. In this preliminary study the placement was chosen based on past experience and no special attempt was made to optimize the configuration. Only three transponder locations were used, these being selected so that, in the course of the flight, the range measurements would give reasonably good information in all three coordinates. However, more advanced versions of the precision ranging systems are available which can use additional transponders. Use of the additional capability would allow selection of a transponder configuration which would overcome line-of-sight difficulties and at the same time provide a more favorable geometry from a navigation point of view. Such a change in configuration, as has been shown by other simulation results, would produce a minor effect on the results presented.

Only a single microwave elevation scanner is shown in Figure 2. In an actual SSV application an additional elevation scanner would probably be employed, but such a change in configuration should have only a minor effect on the results presented here.

Data Rates. The simulation assumed that external measurements were sampled and processed by the Kalman filter every two seconds. This cycle rate, which was imposed on this study by temporary operational limitations in the simulation program, is slower than one would normally use in an actual on-board computer which, with modern computer technology, could conceivably be once every 1/2 second. If the higher filter cycle rate had been used to obtain the results presented here, a slight improvement would have been obtained in most cases.

Filter Initialization. Large initial uncertainties can cause convergence difficulty in the Kalman filter because of measurement nonlinearities. In order to circumvent this problem in an actual system the program must have a built-in "data-start" procedure which computes initial position estimates from data (external measurements) prior to processing any further external measurements with the Kalman filter. In this study, errors were used for the initial position and velocity estimates which would be typical for a "data-start" initialization procedure, as follows:

Component	Error
X	-58.43 ft
Y	46.74 ft
Z	17.12 ft
$\dot{X}$	44.89 ft/sec
$\dot{Y}$	-40.00 ft/sec
$\dot{Z}$	-17.29 ft/sec

RESULTS AND DISCUSSION

The cases considered in this study are as follows:

Figure	Ground Navigation Aid	Data Dropout Time Before Touchdown	Baro Altimeter Data Dropout Time Before Touchdown
3	PRS	0	0
4	PRS	50 sec	0
5	PRS	100 sec	0
6	PRS	100 sec	100 sec
7	MSB	0	0

For each case given in the Table above, five Monte-Carlo runs were made. Each of these runs used the same initial conditions and the same errors which were not estimated.

The random components of the measurements were independent random numbers with a Gaussian distribution about a zero mean. The data presented in the figures are plotted every ten seconds instead of every two seconds to increase the readability of the figures. For each position and velocity component, five Monte-Carlo samples are given in addition to the Kalman filter "system standard deviation" shown as a cross-hatched envelope on each figure. The fact that many points of the Monte-Carlo runs lie outside the envelope is due primarily to the errors which were not estimated and indicates the possible need to modify the pseudo-random forcing function inputs to better "tune" the Kalman filter.

The results of all cases presented in figures 3 through 7 are summarized as RMS errors at touchdown in Table III. These values include not only the spread due to random measurement errors, but also the additional spread which would result if the errors which were not estimated (i.e., biases, etc.) had been randomly selected. The two primary results are shown in the columns for which ground navigation aid data and barometric altimeter data were available to touchdown. These results indicate that navigation performance with either system is adequate for landing the space shuttle orbiter. The greater position error of the microwave scanning beam, particularly in Y, is due primarily to the assumed 1 mr bias of the azimuth scanner. This error is not part of the model given in Reference 3, but is felt to be a realistic value resulting from installation inaccuracies. The X error is due primarily to the 75 foot RMS error in the DME associated with the scanning beam system.

The two runs shown in Table III for PRS data dropout at 50 and 100 seconds prior to touchdown still show acceptable touchdown accuracies. The primary contributors to the increased X and Y position errors were the velocity errors and errors in the estimated tilts at the time of data dropout. The good position and velocity estimates in the Z axis are due to the fact that the barometric altimeter had become well calibrated prior to data dropout, and it remained as an accurate data source.

Without the barometric altimeter, or some other source of data containing altitude information, the Z axis position and velocity estimates from the INS are unstable. The effect of this instability can be seen in Table III for the case where the barometric altimeter data was dropped at 100 seconds, along with the PRS data. Although the X and Y position estimates remain useable, the Z axis position error becomes unuseably large for automatic touchdown purposes. It may be useable for approach in Category II visibility conditions, however.

Table III also shows the RMS errors at touchdown for the case where the PRS was used all the way to touchdown but no barometric altimeter data was included. Plots of the five Monte Carlo position and velocity components were not included for this case because their basic form is similar to those presented in figure 3 except that a change in scales would be required for all but the $\dot{X}$ component. These data indicate that on this trajectory the PRS alone was capable of providing reasonably good navigation accuracy at touchdown.

REFERENCES

1. North American Rockwell, Aerodynamic Design Data Book DB 2.1.4-13000-10; 9992-134D, "Configuration Layout Delta Wing SSV Orbiter", dated September 1, 1970.

2. Robinson, G.G. and Johnson, N.S.: "Subsystem Requirements for an Airborne Laboratory to Study Zero-Zero Landing Systems". Ames Research Center, Moffett Field, California. Presented at the 25th Meeting of Flight Mechanics Panel of Advisory Group for Aeronautical Research and Development, Munich, Germany; October 12-14, 1964.

3. Cherry, G.N., et al.: "Space Shuttle Trajectory Management, Navigation, Guidance and Control During Approach and Landing". Charles Stark Draper Laboratory, M.I.T. Appendix D, Interim Report No. R 667, May 1970.

TABLE I - IMU ERRORS

	Uncertainty (1σ)	Level (3σ)
Alinement (Stellar)	2 Arc Min All Axes	0
Gyro		
g insensitive	.004°/hr	4 deg/hr
g sensitive	.04°/hr	6 deg/hr
*alinement	.3 milliradian	3 milliradians
*scale factor	200 ppm	3000 ppm
Accelerometer		
bias	20 ug	.01g
scale	50 ppm	3000 ppm
*alinement	5 arc sec	60 arc sec
linearity	.005%	

*Factory calibration only.

TABLE II- SENSOR ERROR MODELS

System		Random (1 σ)	Bias
Precision Ranging System		1.5 ft	1 ft
Microwave Scanning Beam	Azimuth	.5 mr	1 mr
	Elevation	.5 mr	1 mr
	Range	75 ft	10 ft
Baro-Altimeter		2 ft	10 ft +4 ft hystersis

TABLE III - RMS ERRORS AT TOUCHDOWN

	Precision-Ranging System Data Dropout: Time Before Touchdown (Baro-Alt. data always available)			PRS and Baro-Alt. Data Dropout at -100 sec	MICROWAVE SCAN BEAM DATA Plus Baro Altimeter	PRS Data to Touchdown No Baro. Alt. Data
	0 sec	50 sec	100 sec			
X	1.5 ft	5 ft	15 ft	15 ft	20 ft	2.5
Y	1.5 ft	7 ft	15 ft	15 ft	30 ft	3.0
Z	1.5 ft	1.5 ft	1.5 ft	10 ft	2 ft	4.5
$\dot{X}$	.05 ft/sec	.15 ft/sec	.15 ft/sec	.2 ft/sec	.6 ft/sec	.05
$\dot{Y}$	.03 ft/sec	.25 ft/sec	.25 ft/sec	.25 ft/sec	.3 ft/sec	.12
$\dot{Z}$	.03 ft/sec	.03 ft/sec	.03 ft/sec	.15 ft/sec	.03 ft/sec	.13

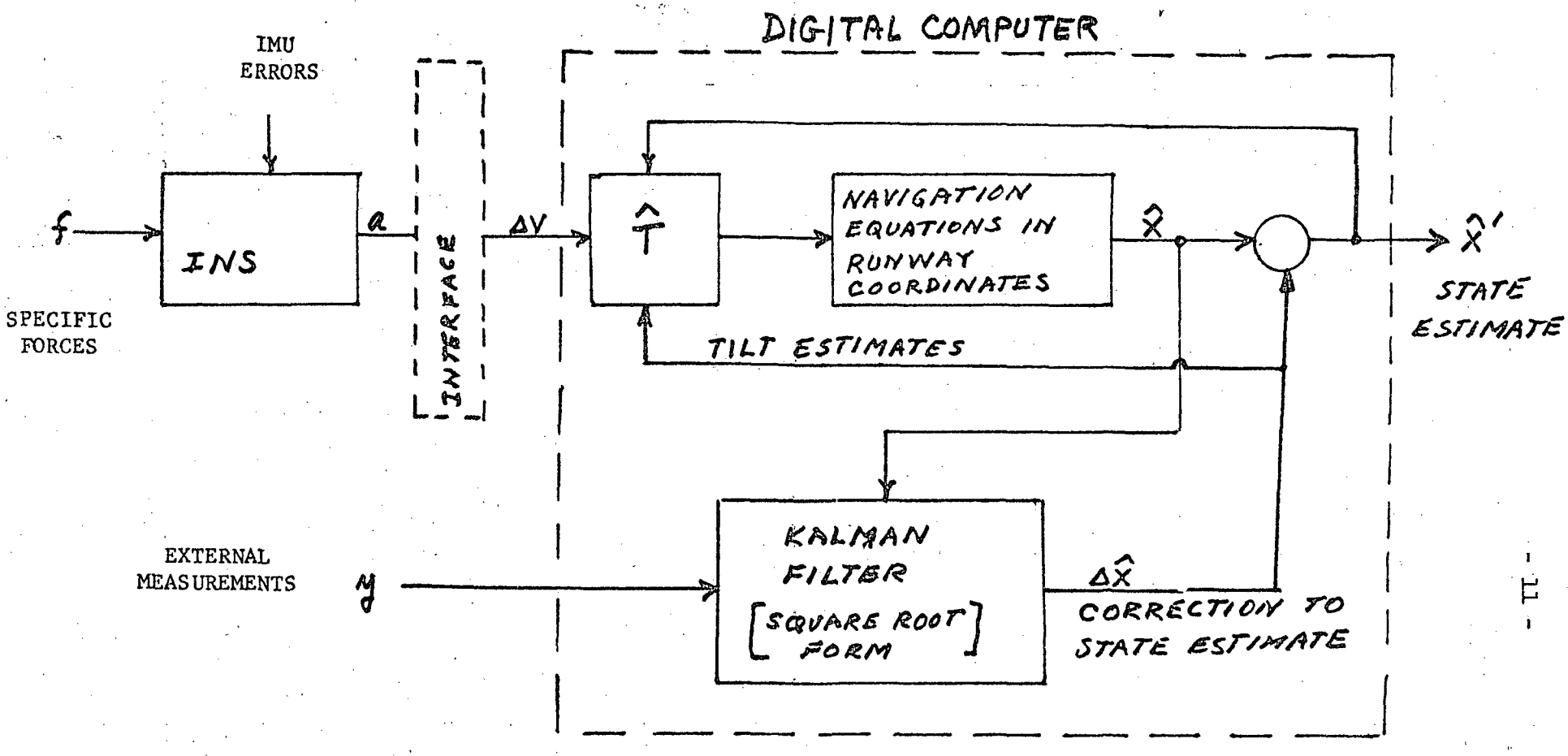

a -- 3 axis accelerometer signals

ΔV -- 3 axis quantized velocity increments

$\hat{T}$ -- total tilt transformation (platform to runway)

$$\hat{x}' = \begin{bmatrix} X \\ Y \\ Z \\ \dot{X} \\ \dot{Y} \\ \dot{Z} \\ \text{TILT 1} \\ \text{TILT 2} \\ \text{TILT 3} \\ \text{VERT ACC BIAS} \\ \text{BARO ALT BIAS} \end{bmatrix}$$

Figure 1 - RAINPAL MECHANIZATION

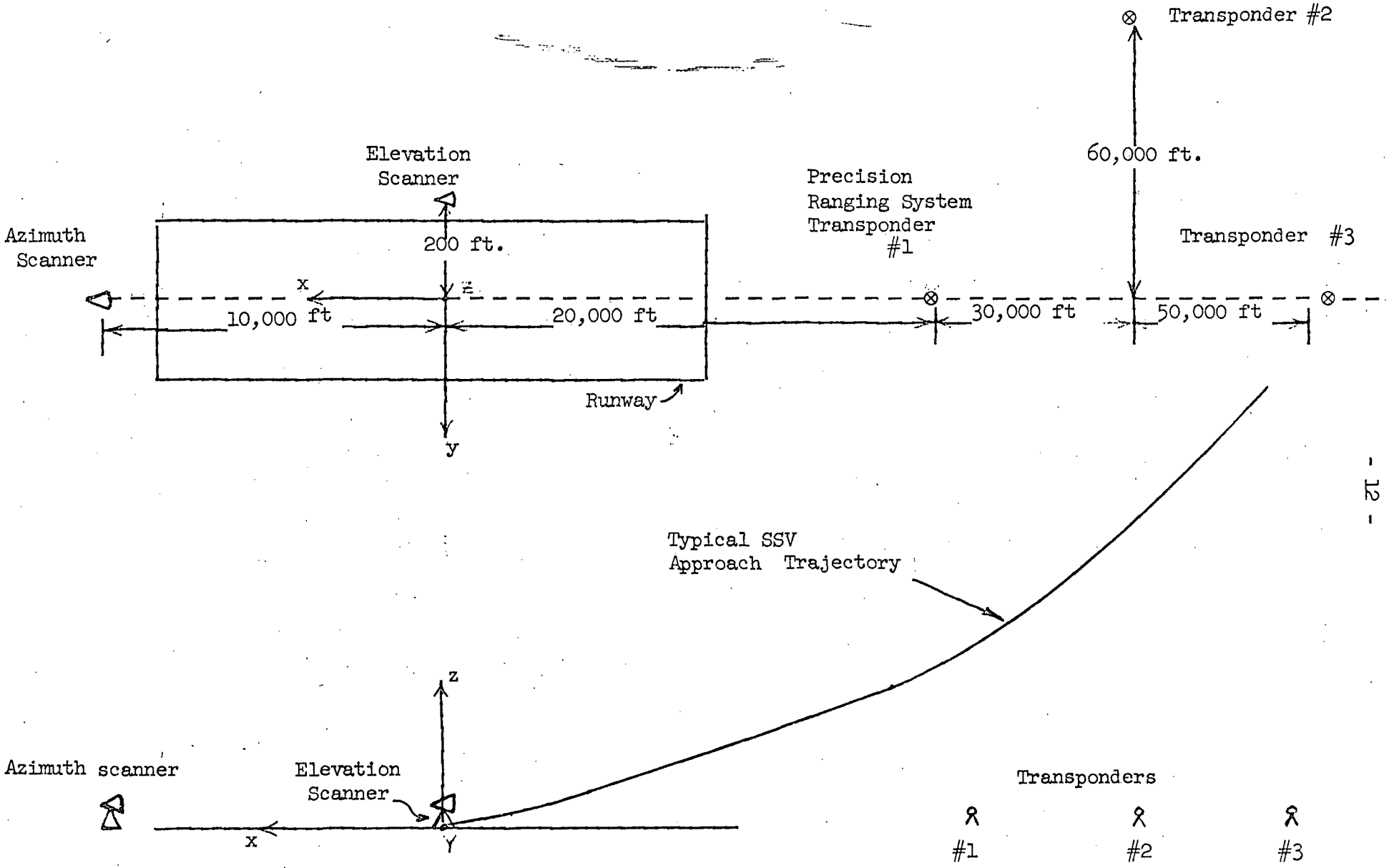

Figure 2 - Location of Ground Navigation Aids Relative to Runway (Not to Scale)

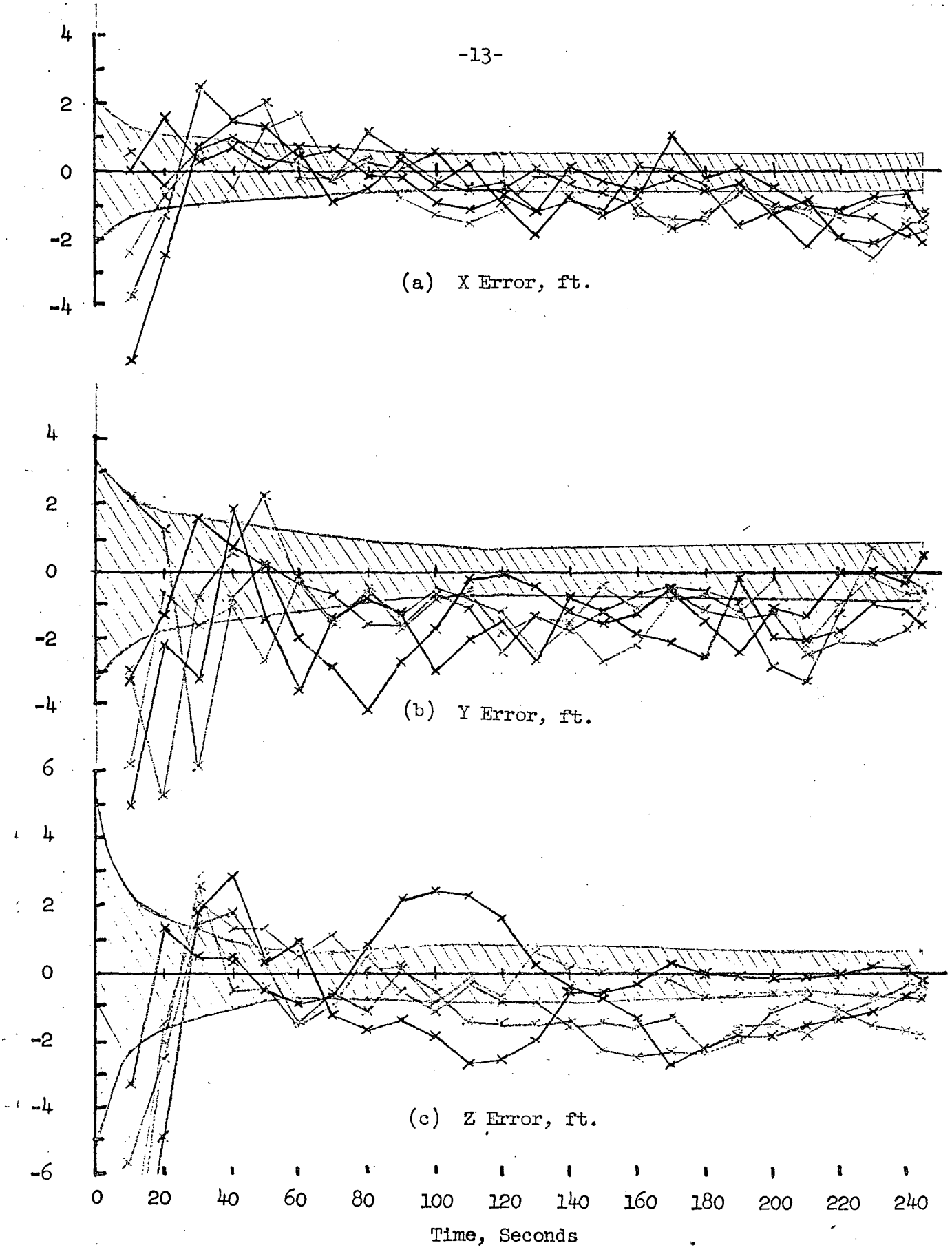

Figure 3 - Time History of Estimation Error, Using Precision Ranging and Baro-Altimeter

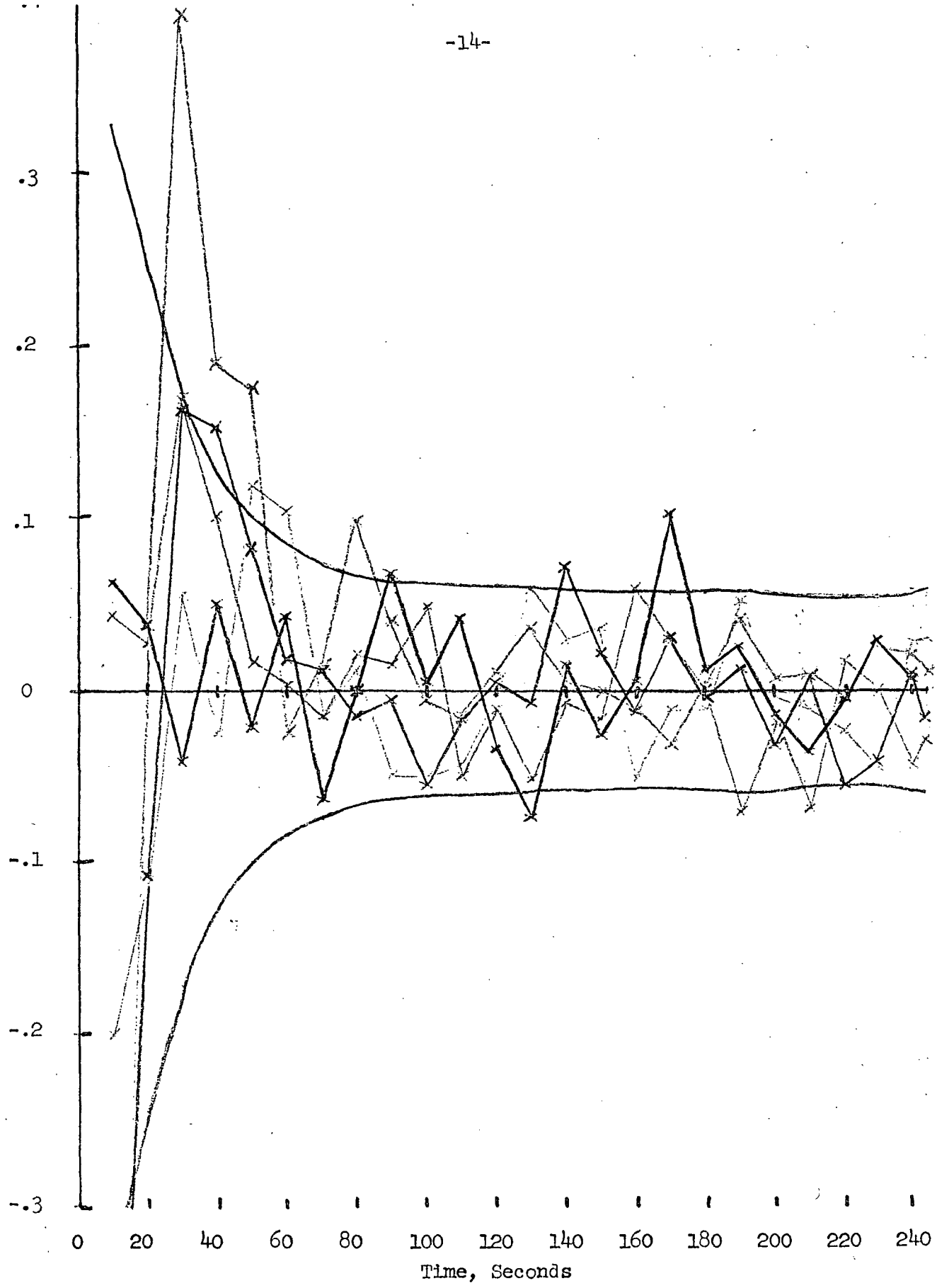

(d) $\dot{X}$ Error, ft/sec

Figure 3 - (cont'd)

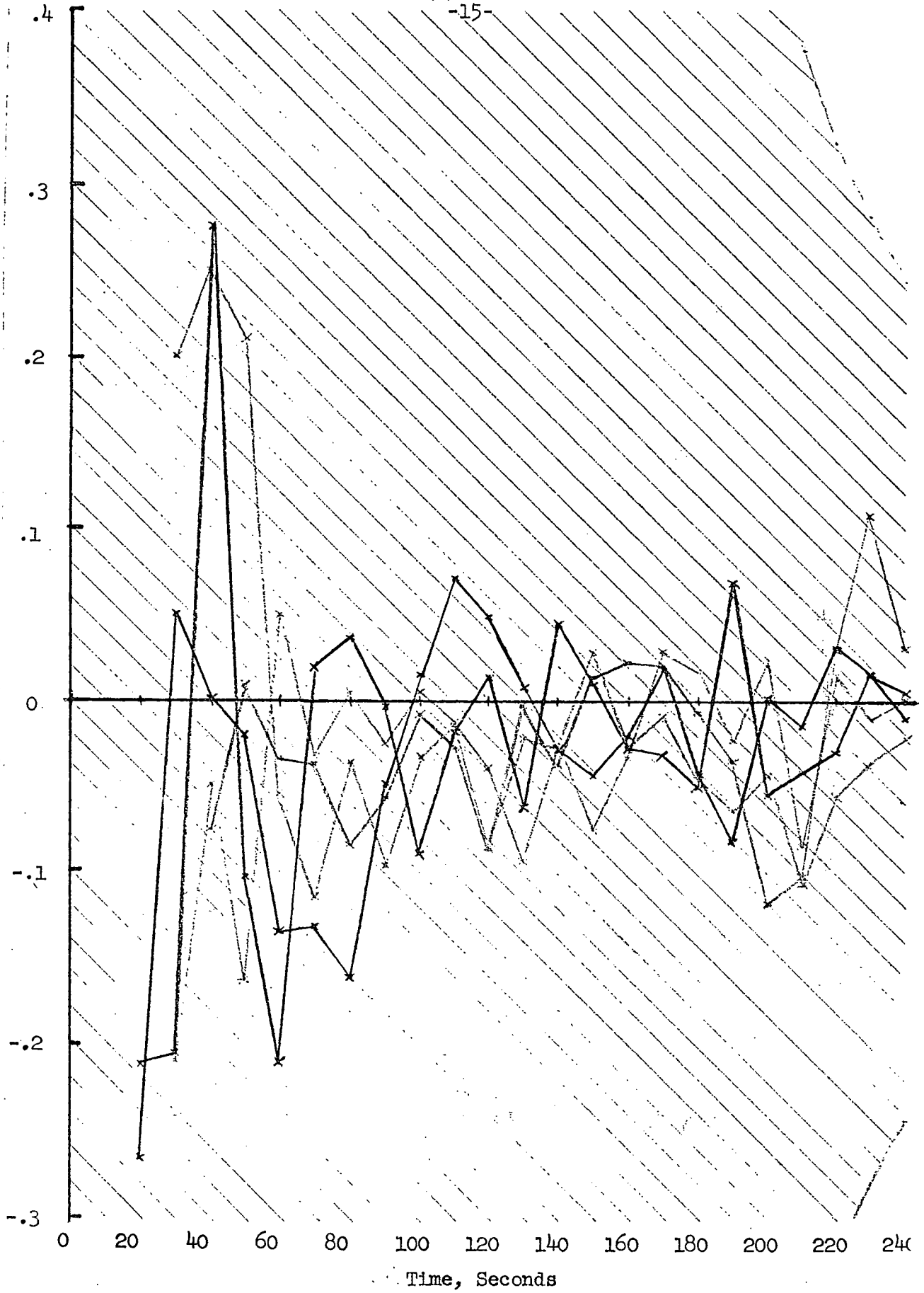

(e) $\dot{Y}$ Error, ft/sec

Figure 3 - (cont'd)

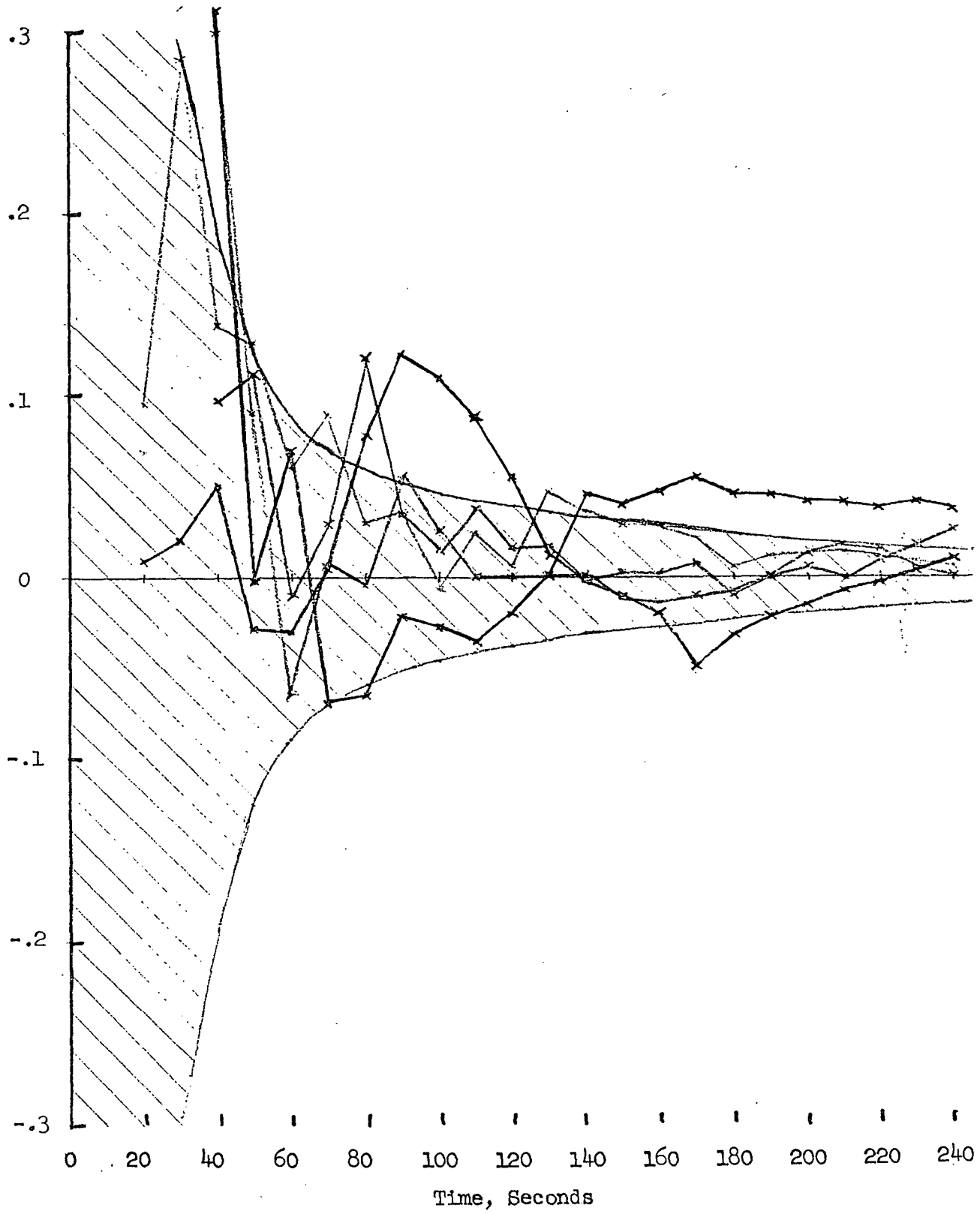

(f) $\dot{Z}$ Error, ft/sec

Figure 3 - (concl.)

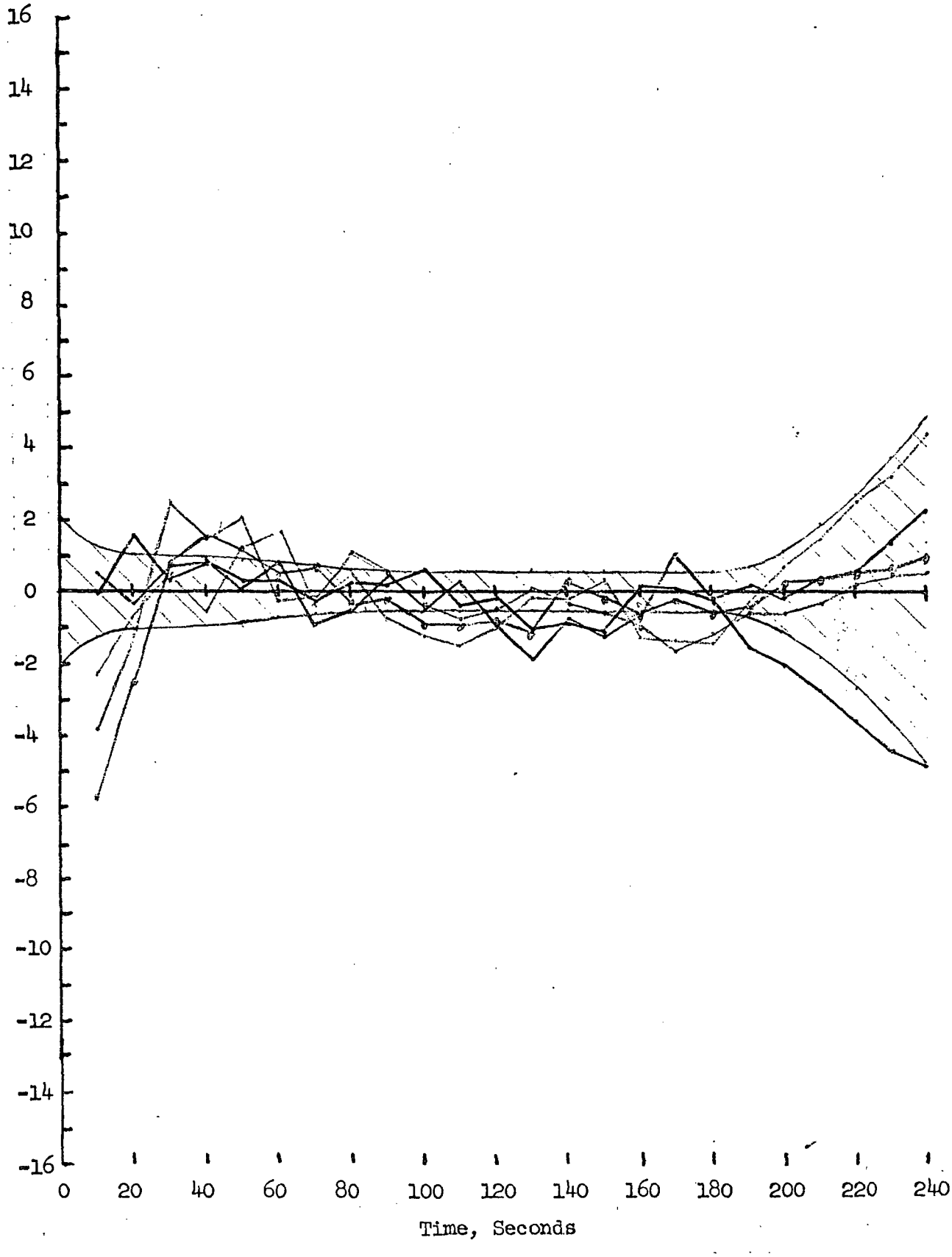

(a) X Error, ft

Figure 4 - Time History of Estimation Error, With Baro-Altimeter Data Always Available, Precision Ranging Data Dropout 50 Seconds Before Touchdown

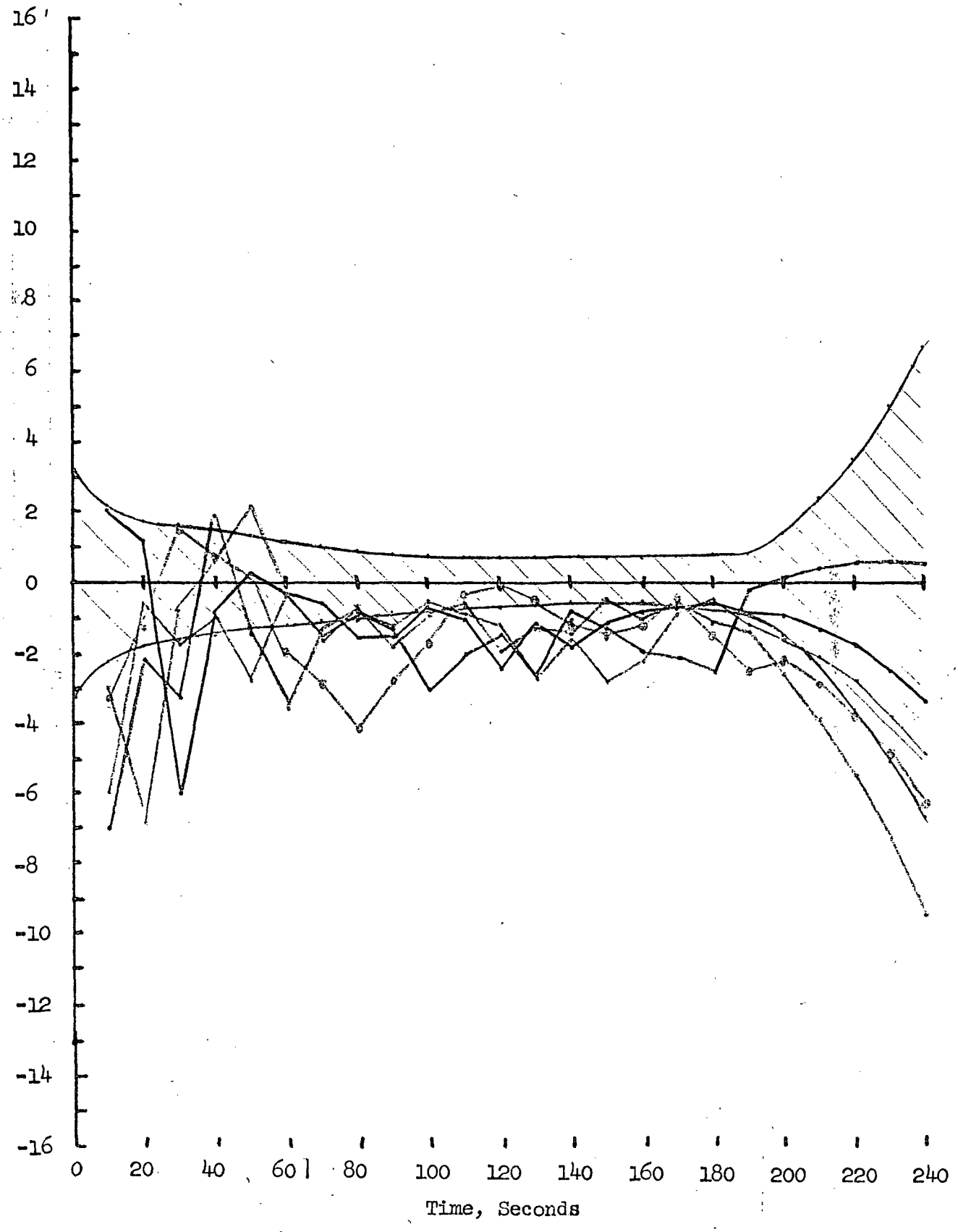

(b) Y Error, ft

Figure 4 - (cont'd)

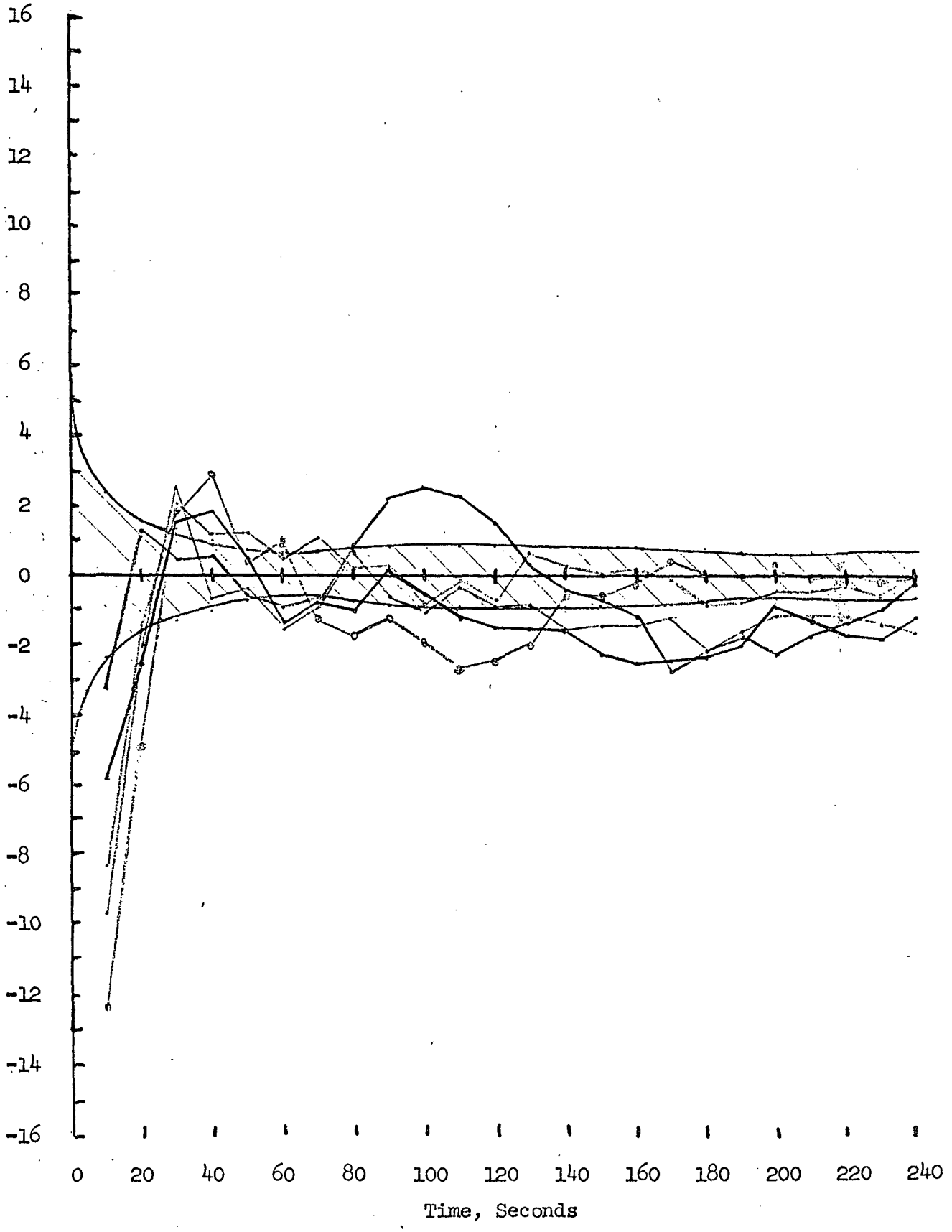

(c) Z Error, ft

Figure 4 - (cont'd)

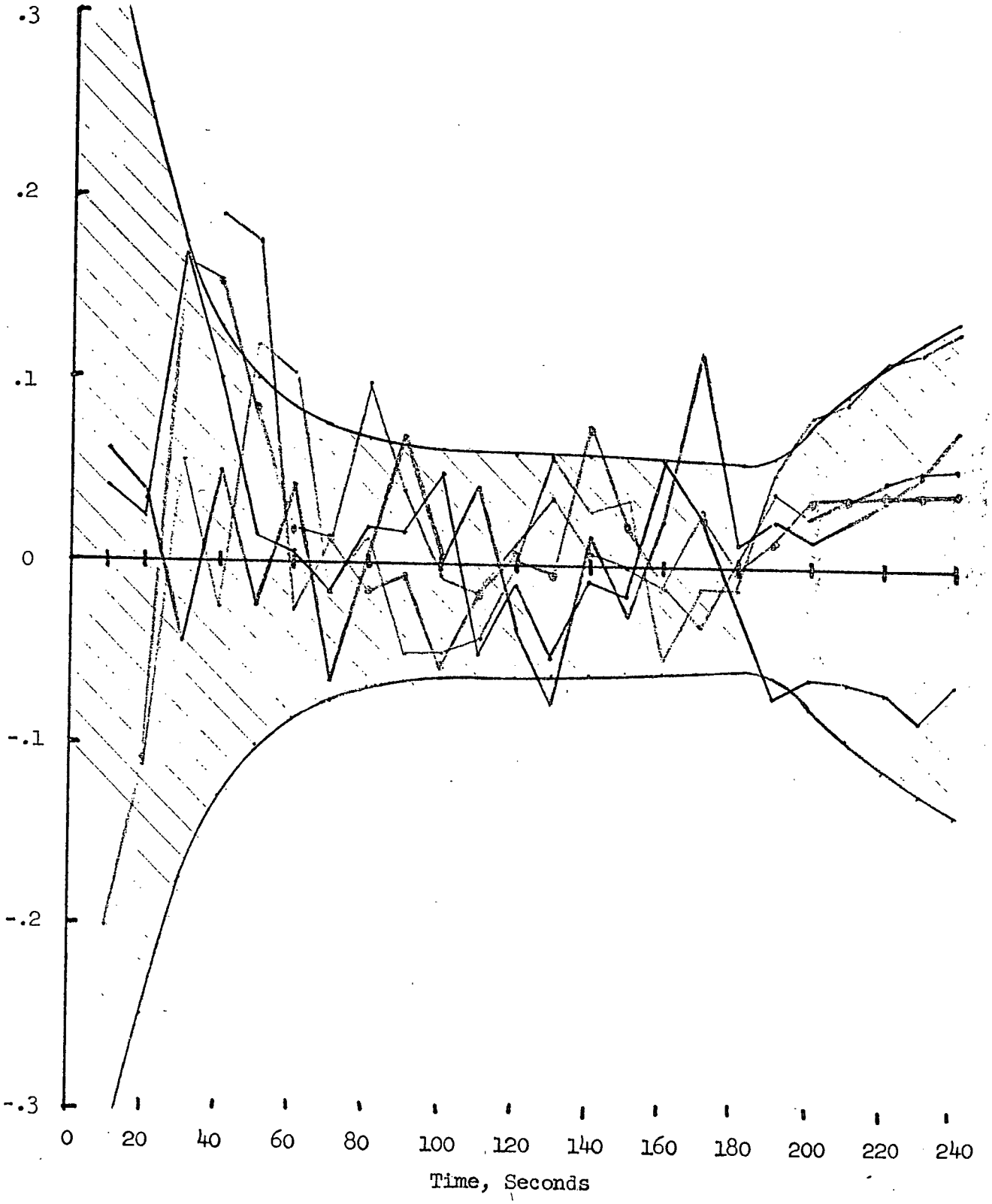

(d) $\dot{X}$ Error, ft/sec

Figure 4 - (cont'd)

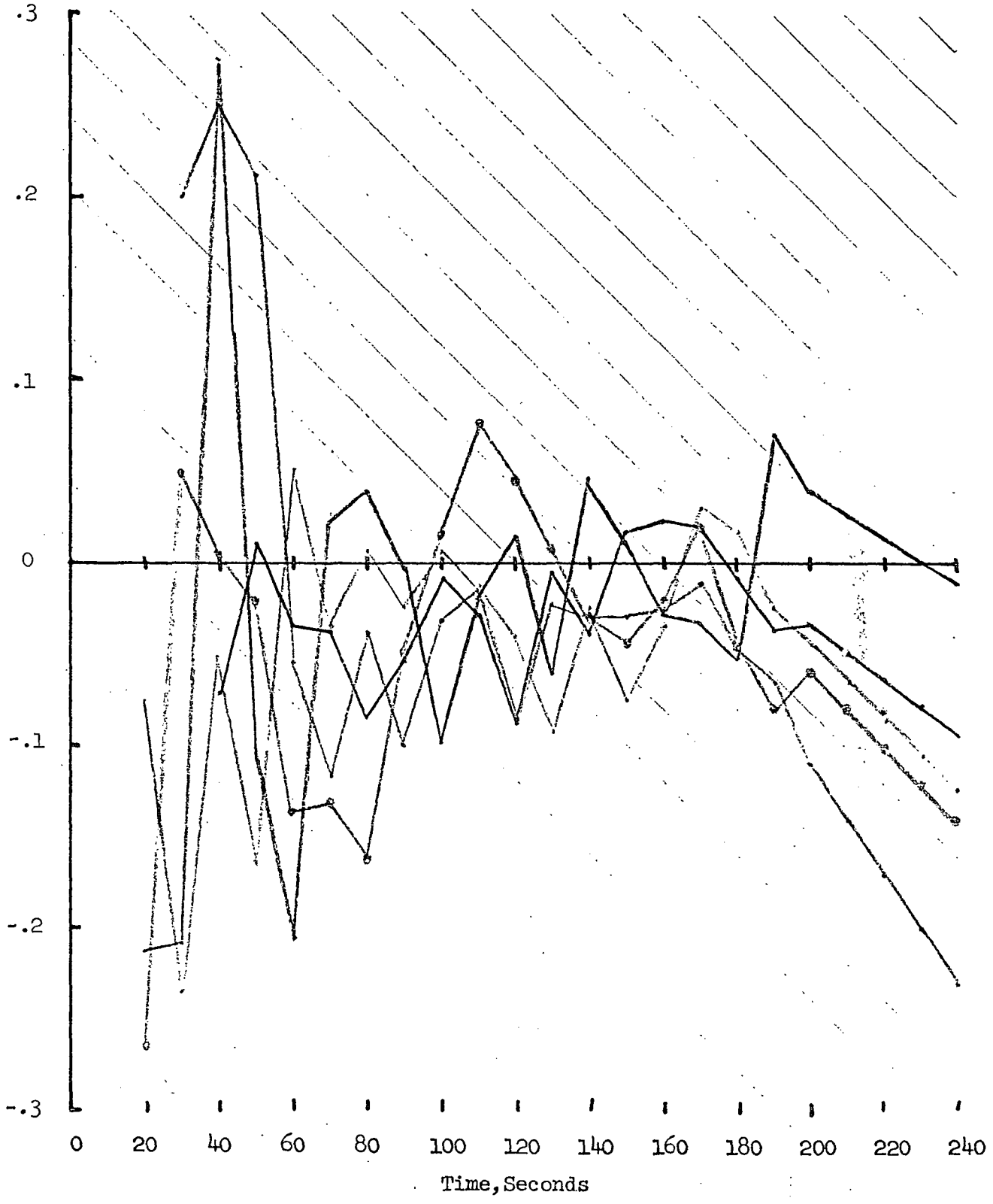

(e) $\dot{Y}$ Error, ft/sec

Figure 4 - (cont'd)

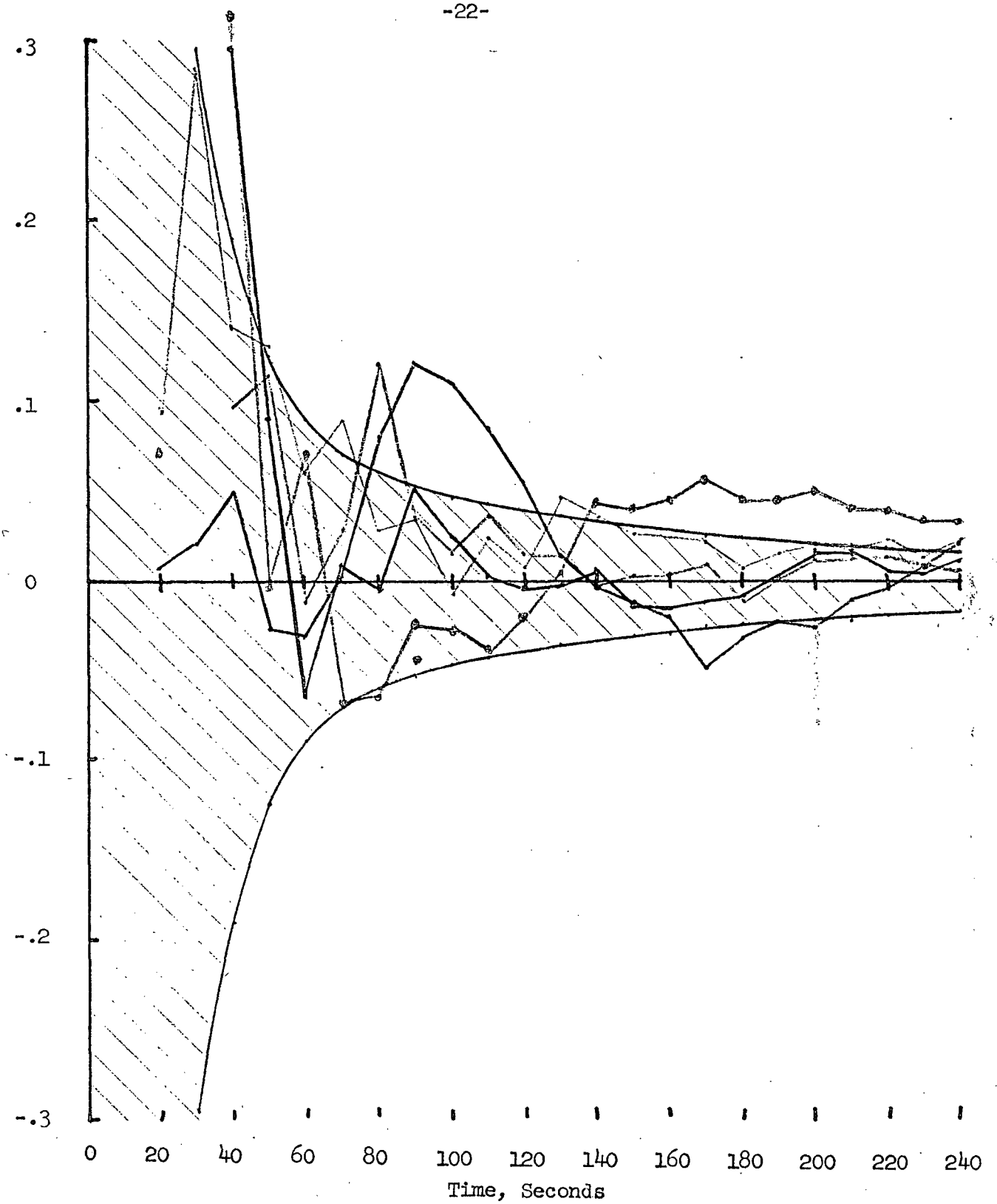

(f) $\dot{Z}$ Error, ft/sec

Figure 4 - (concl.)

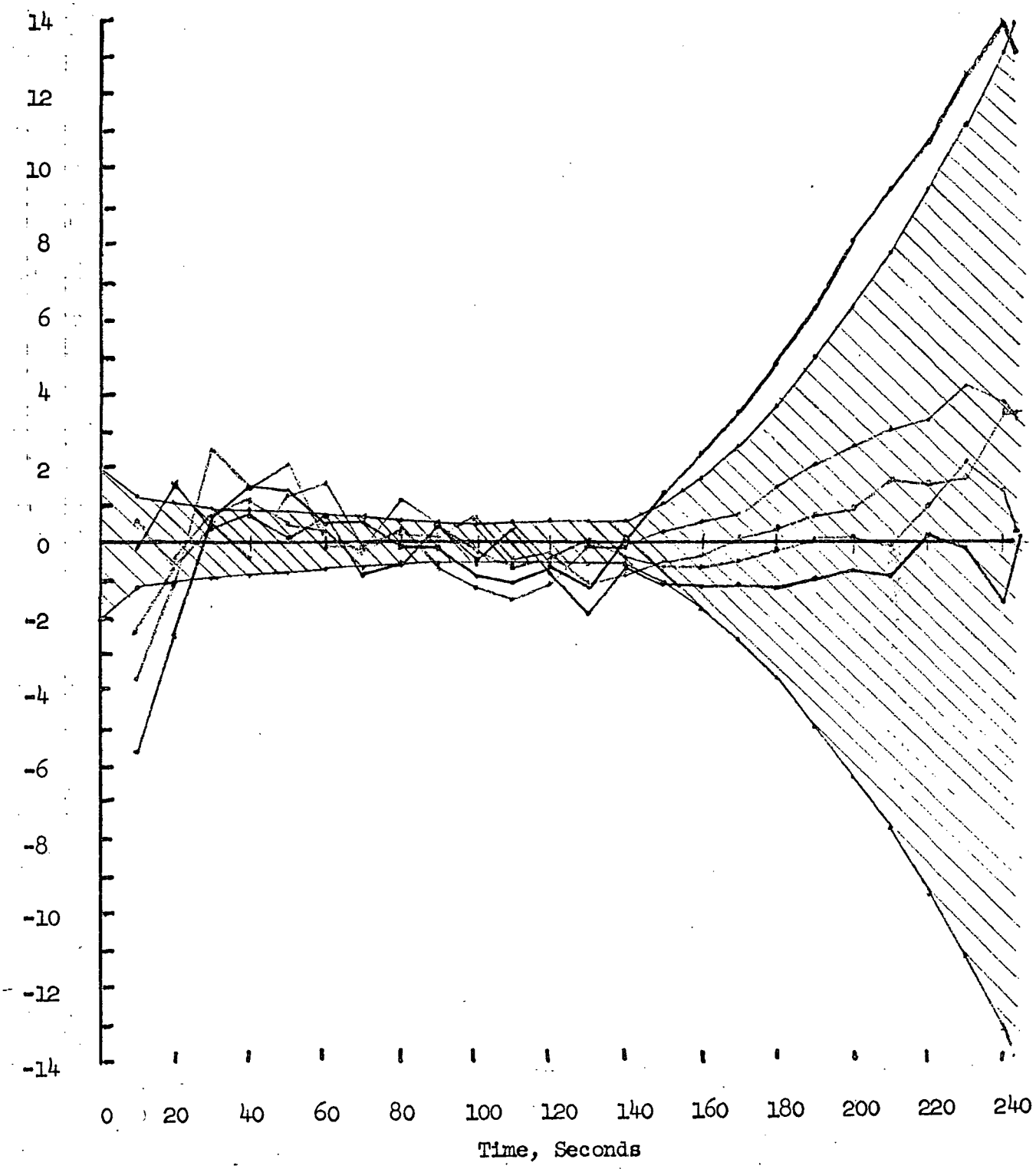

(a) X Error, ft

Figure 5 - Time History of Estimation Error With Baro-Altimeter Data Always Available, Precision Ranging Data Dropout 100 Seconds Before Touchdown

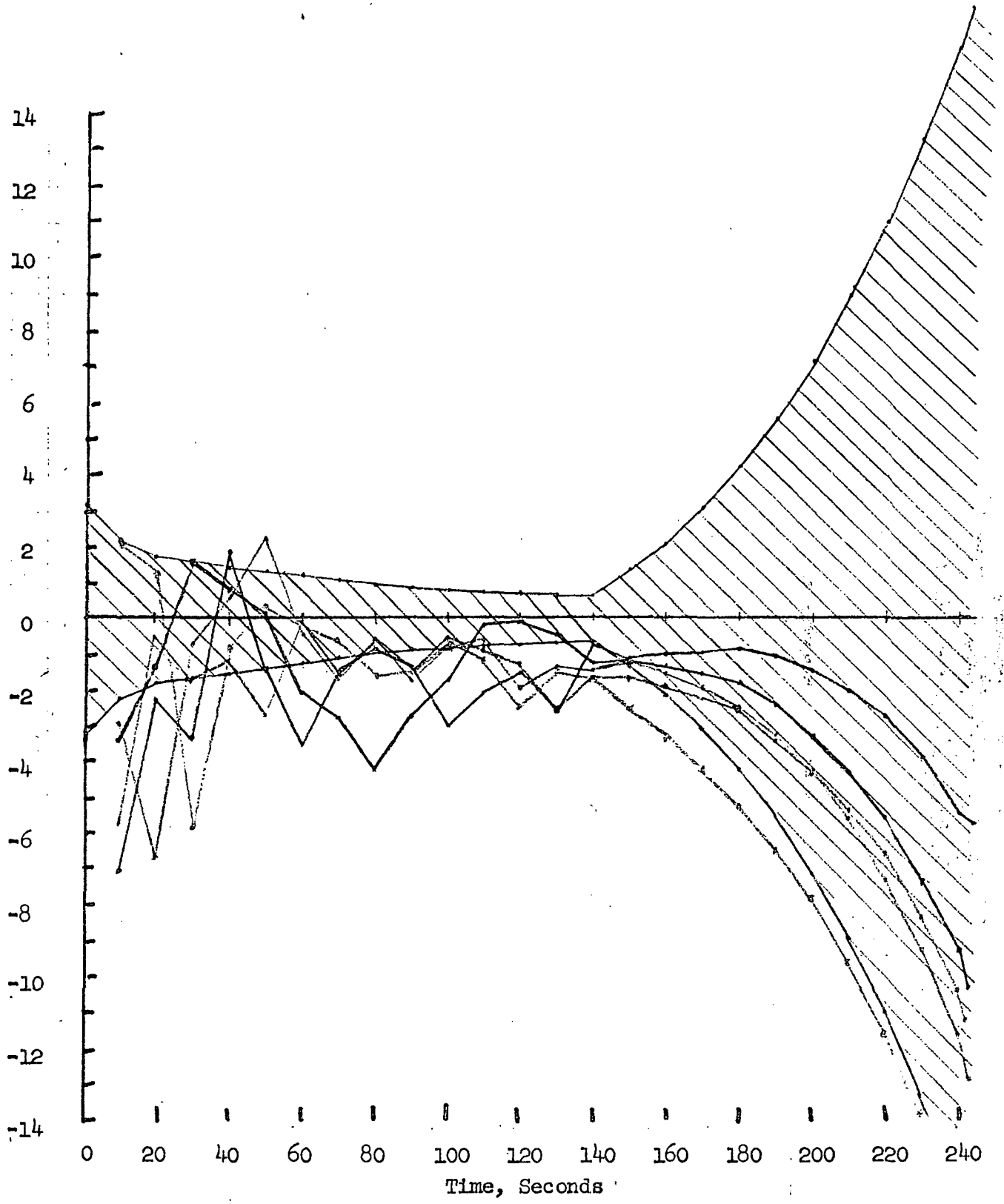

(b) Y Error, ft

Figure 5 - (cont'd)

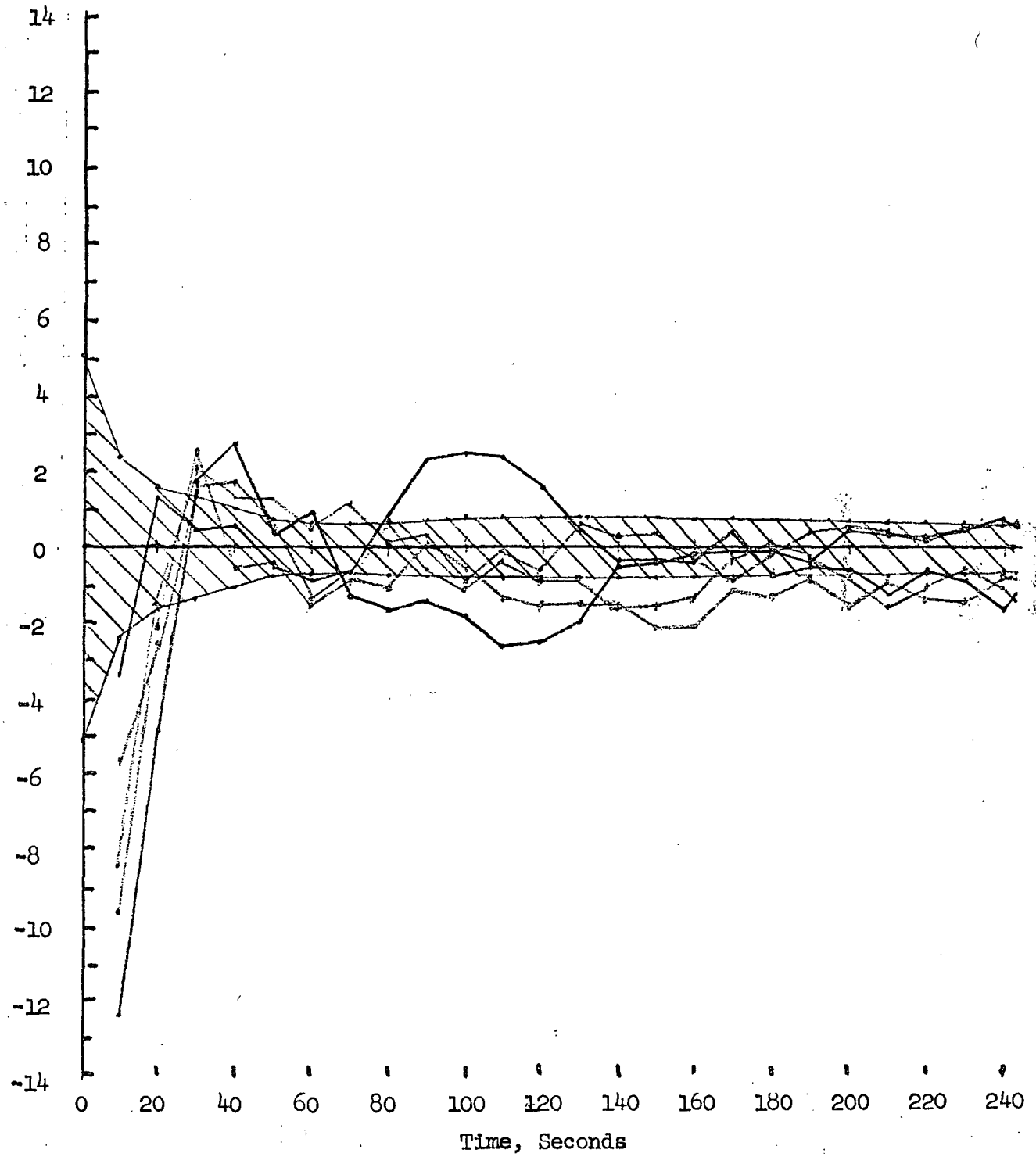

(c) Z Error, ft

Figure 5 - (cont'd)

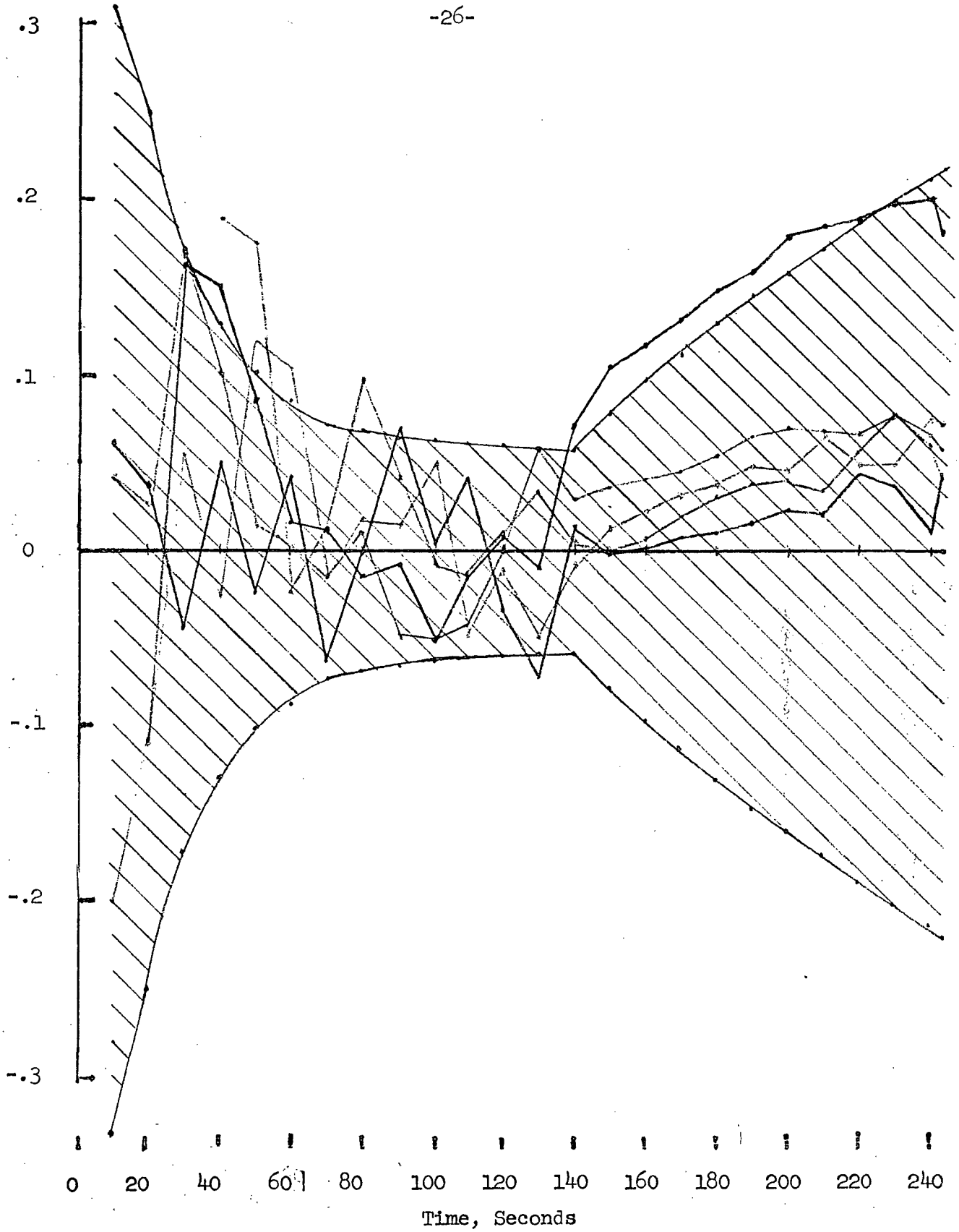

(d) $\dot{X}$ Error, ft/sec

Figure 5 - (cont'd)

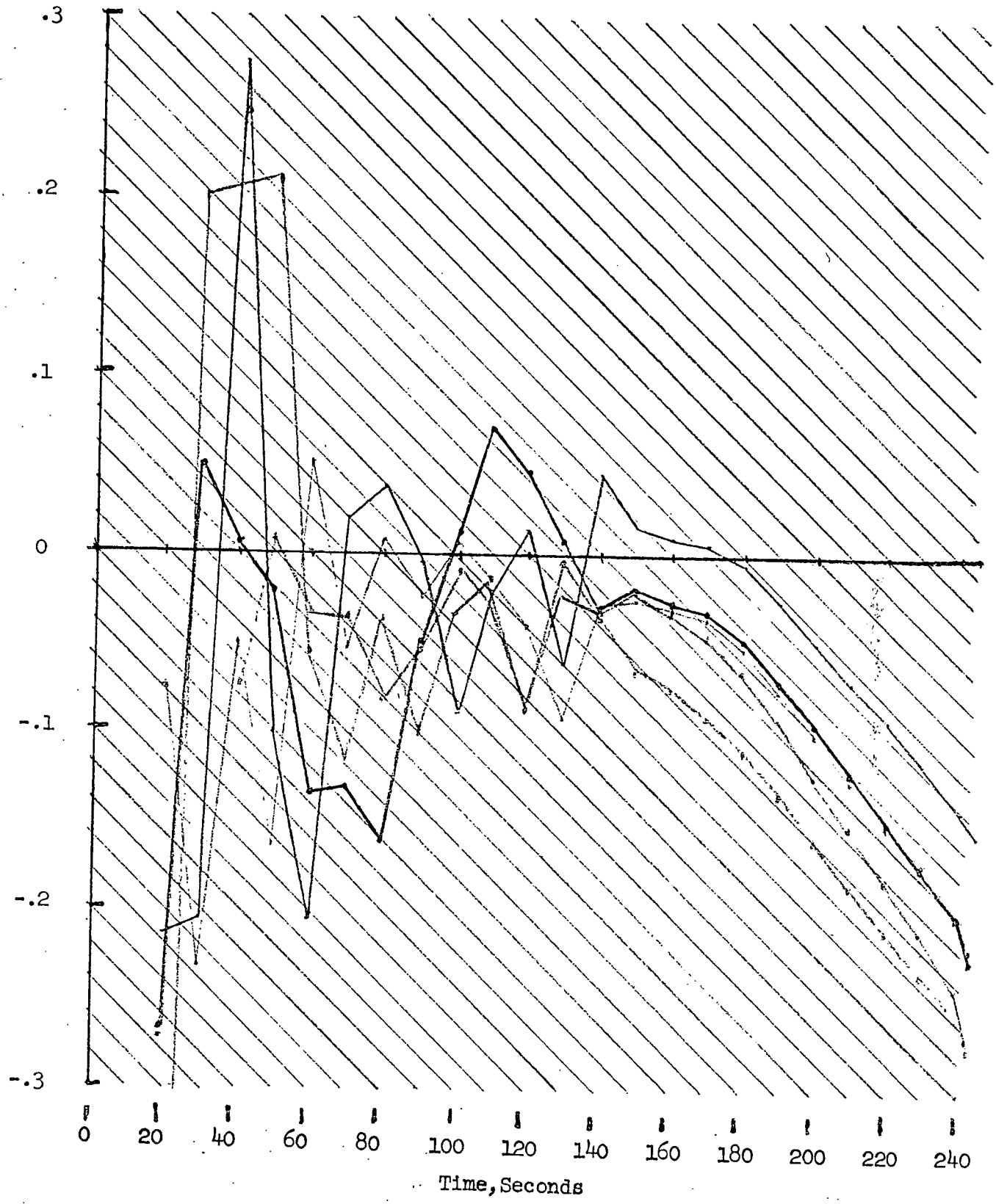

(e) $\dot{Y}$ Error, ft/sec

Figure 5 - (cont'd)

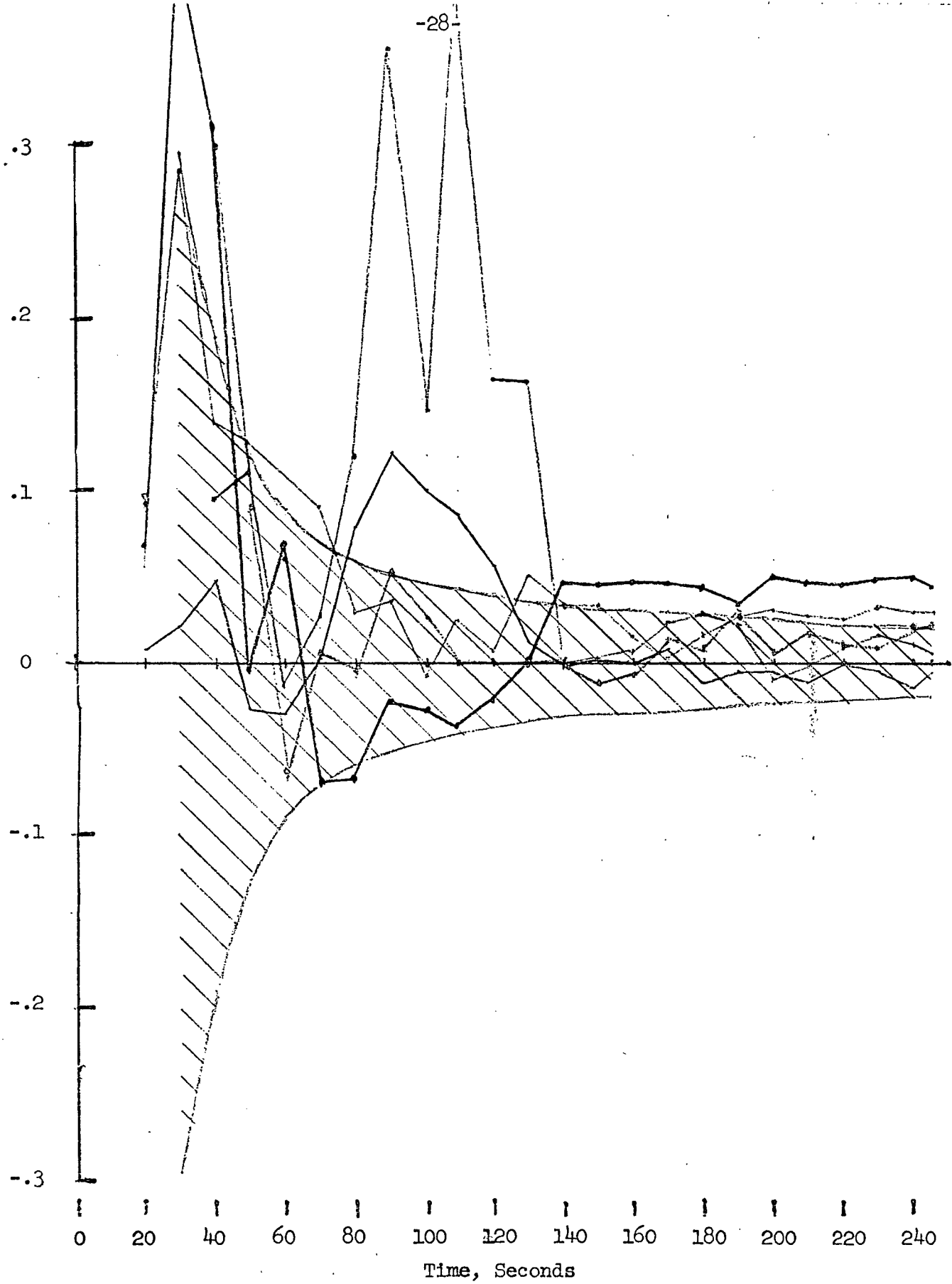

(f) $\dot{Z}$ Error, ft/sec

Figure 5 - (concl.)

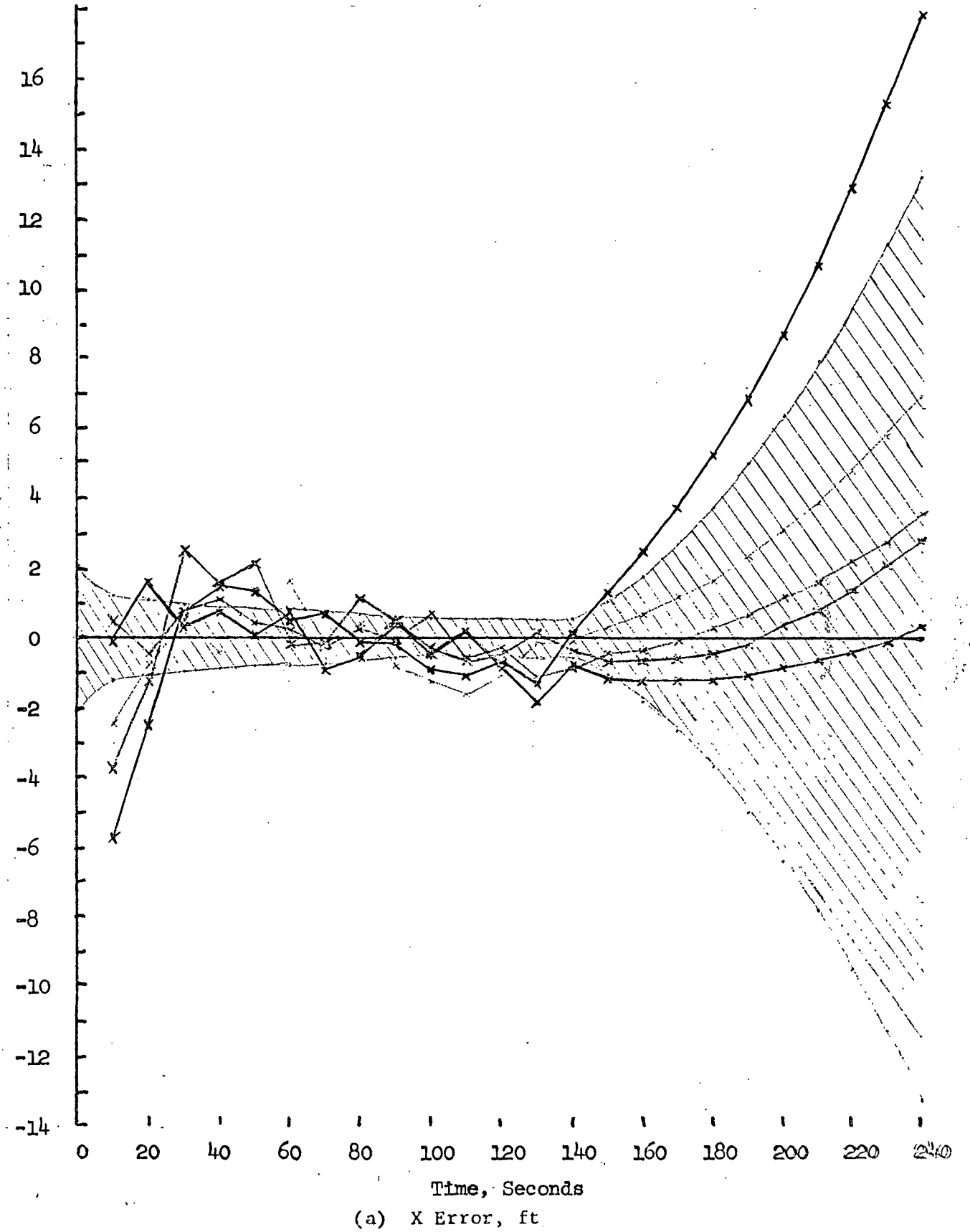

(a) X Error, ft

Figure 6 - Time History of Estimation Error With Precision Ranging and Baro-Altimeter Dropout 100 Seconds Before Touchdown

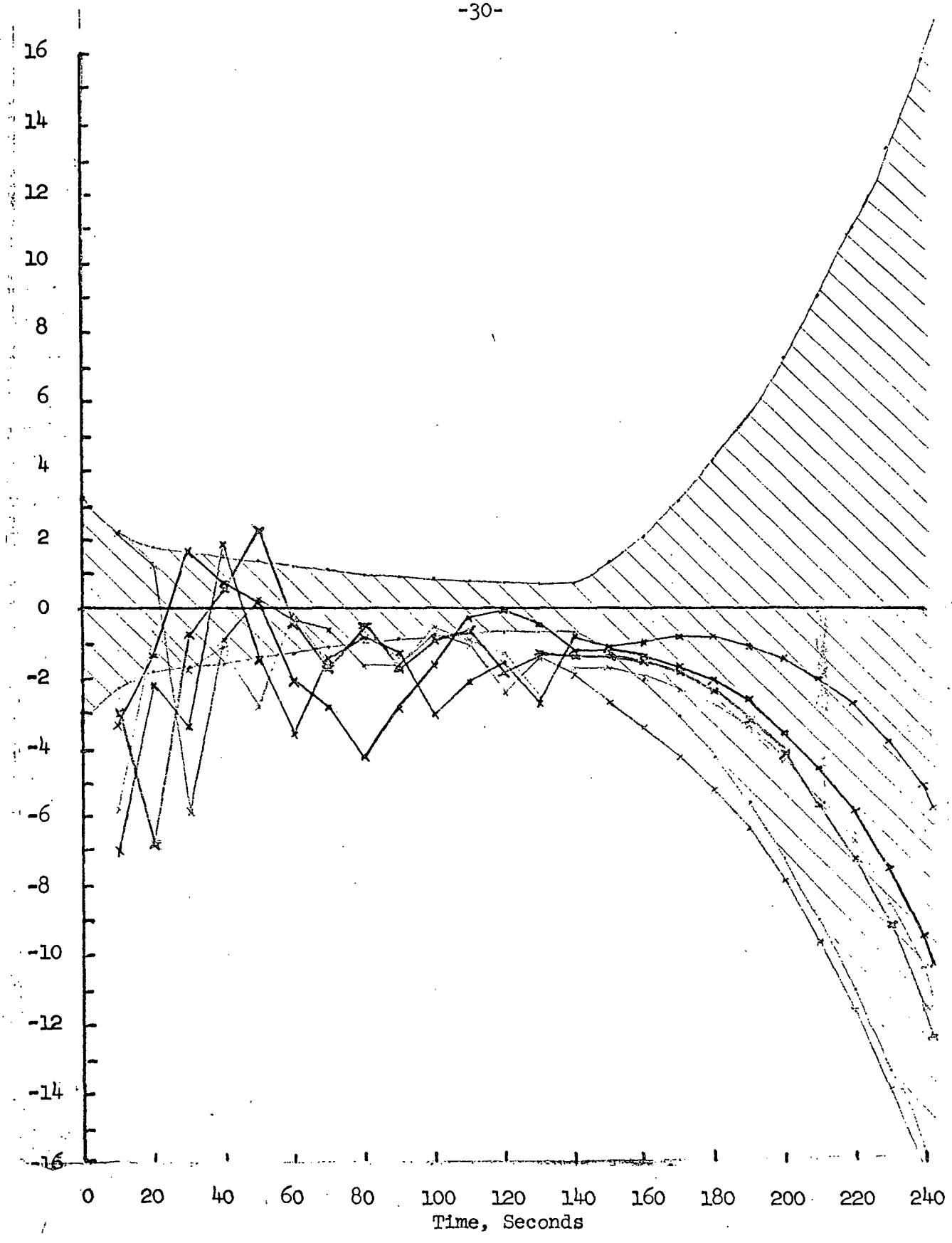

(b) Y Error, ft

Figure 6 - (cont'd)

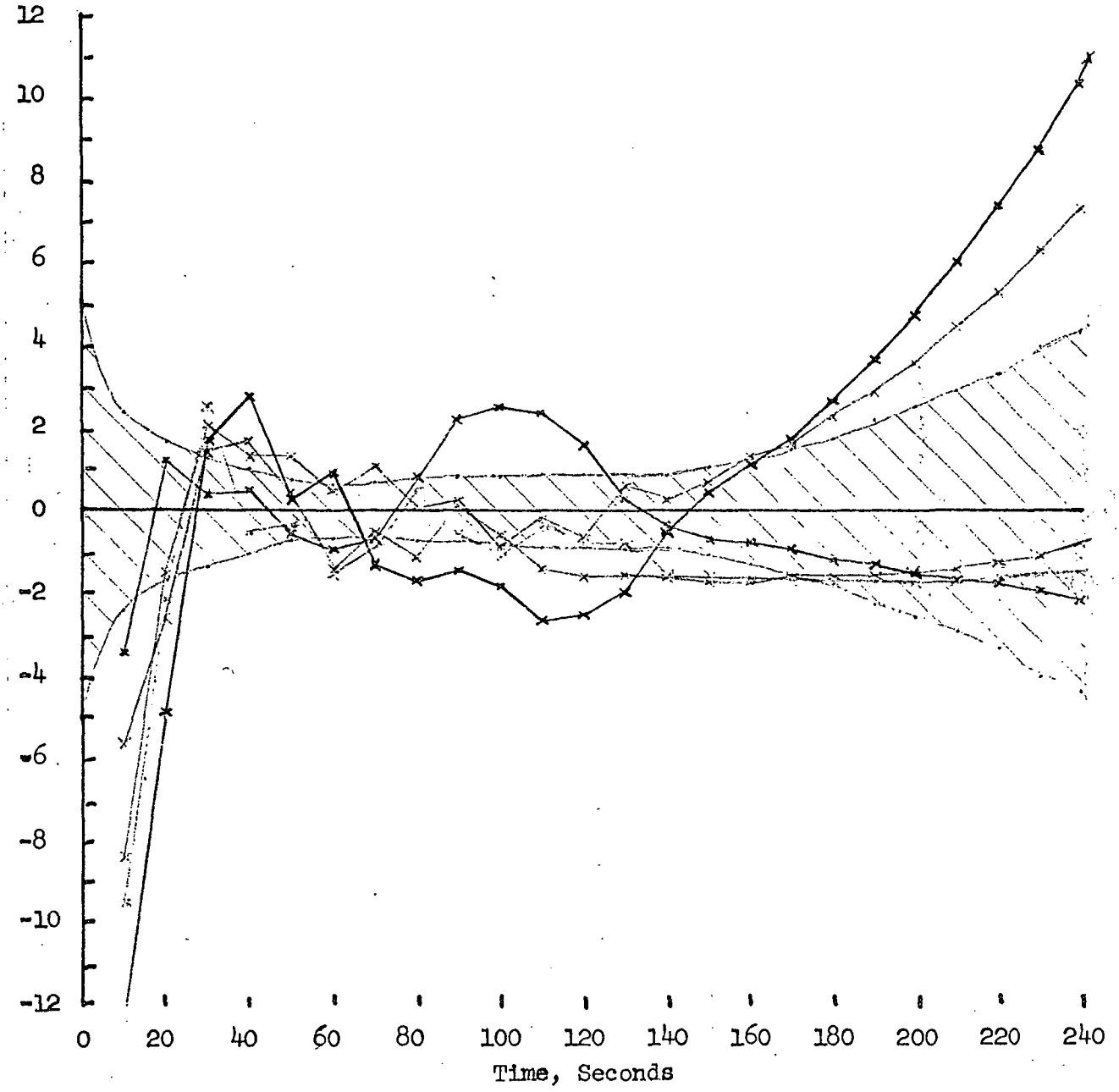

(c) Z Error, ft

Figure 6 - (cont'd)

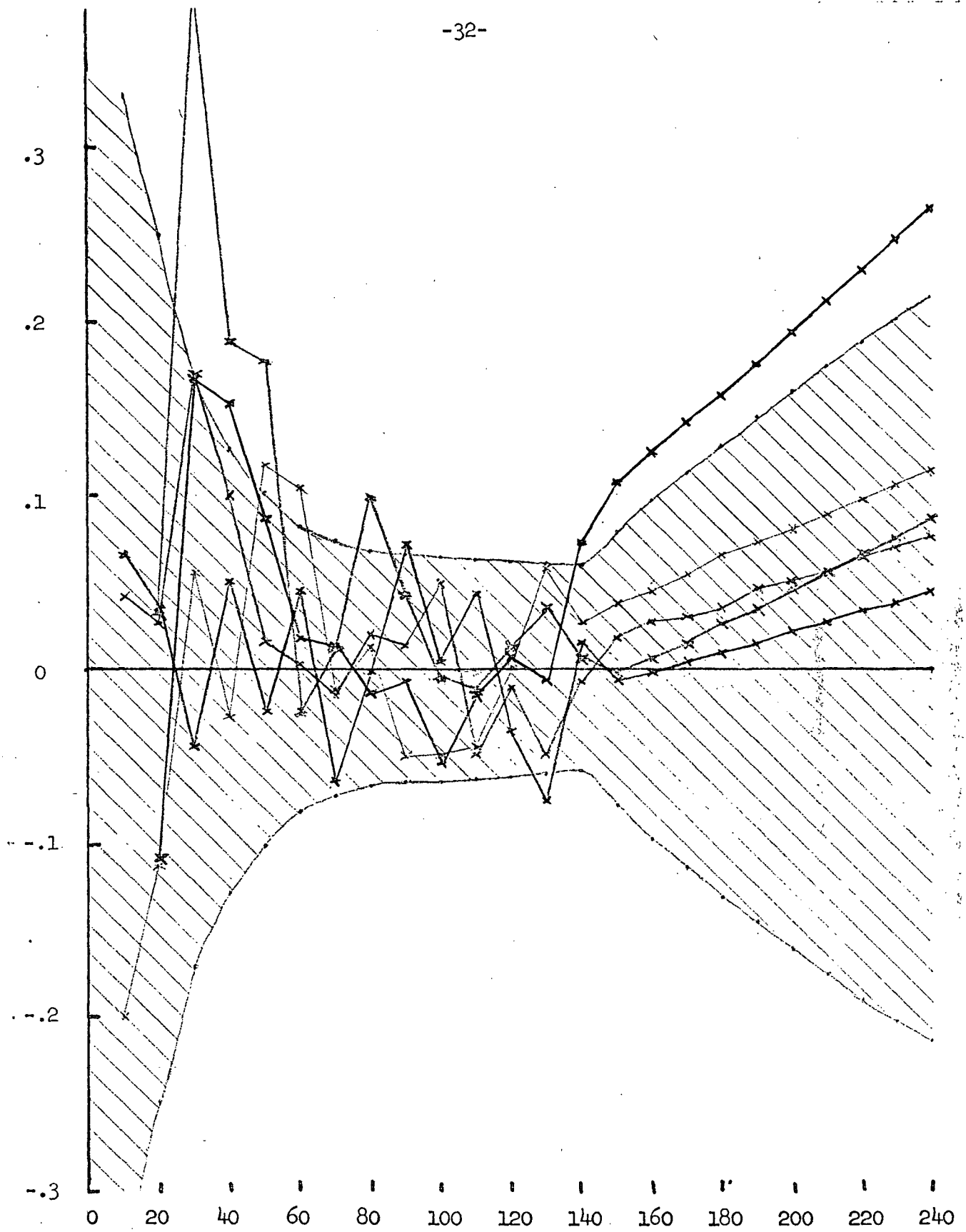

(d) $\dot{X}$ Error, ft/sec

Figure 6 - (cont'd)

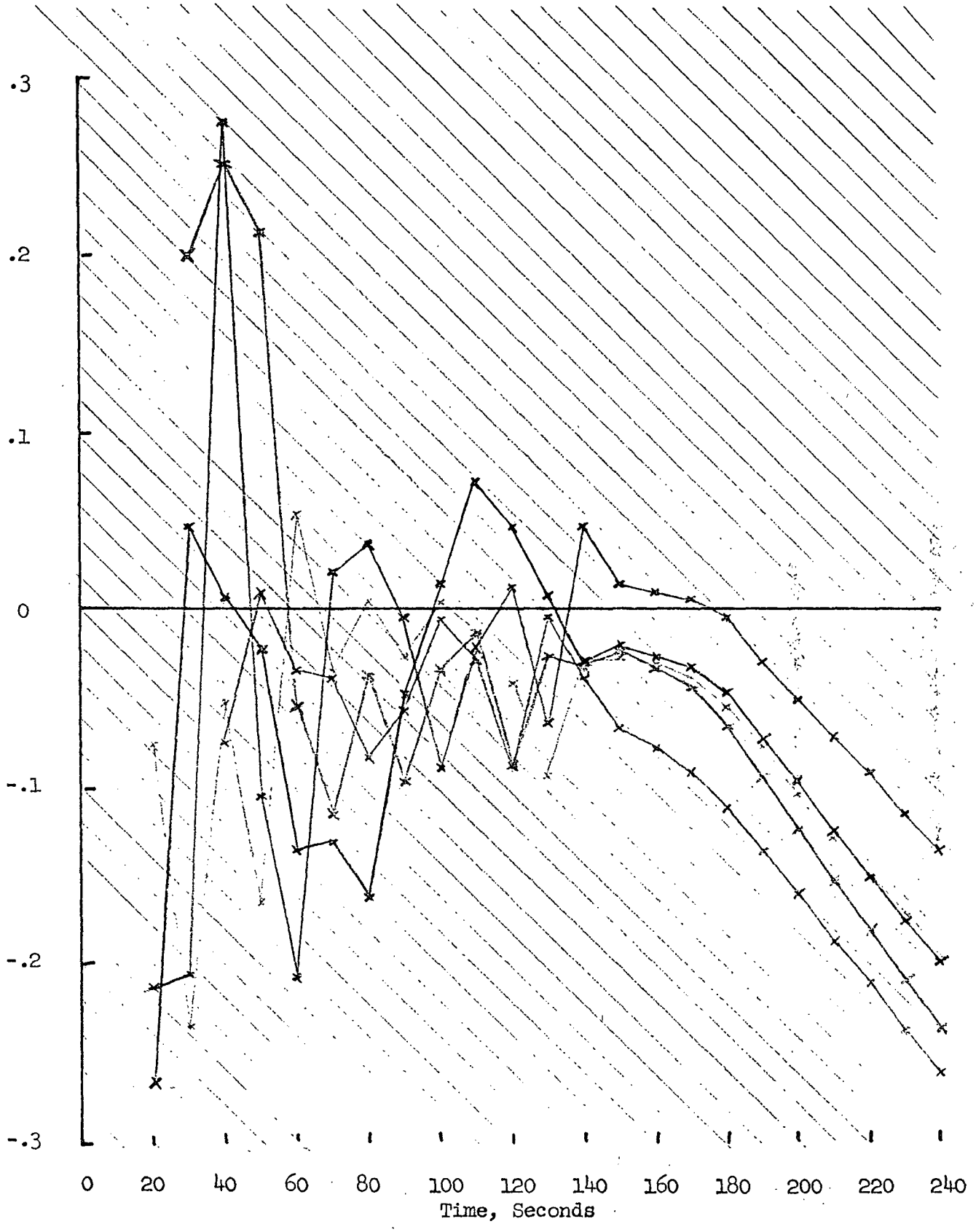

(e) $\dot{Y}$ Error, ft/sec

Figure 6 - (cont'd)

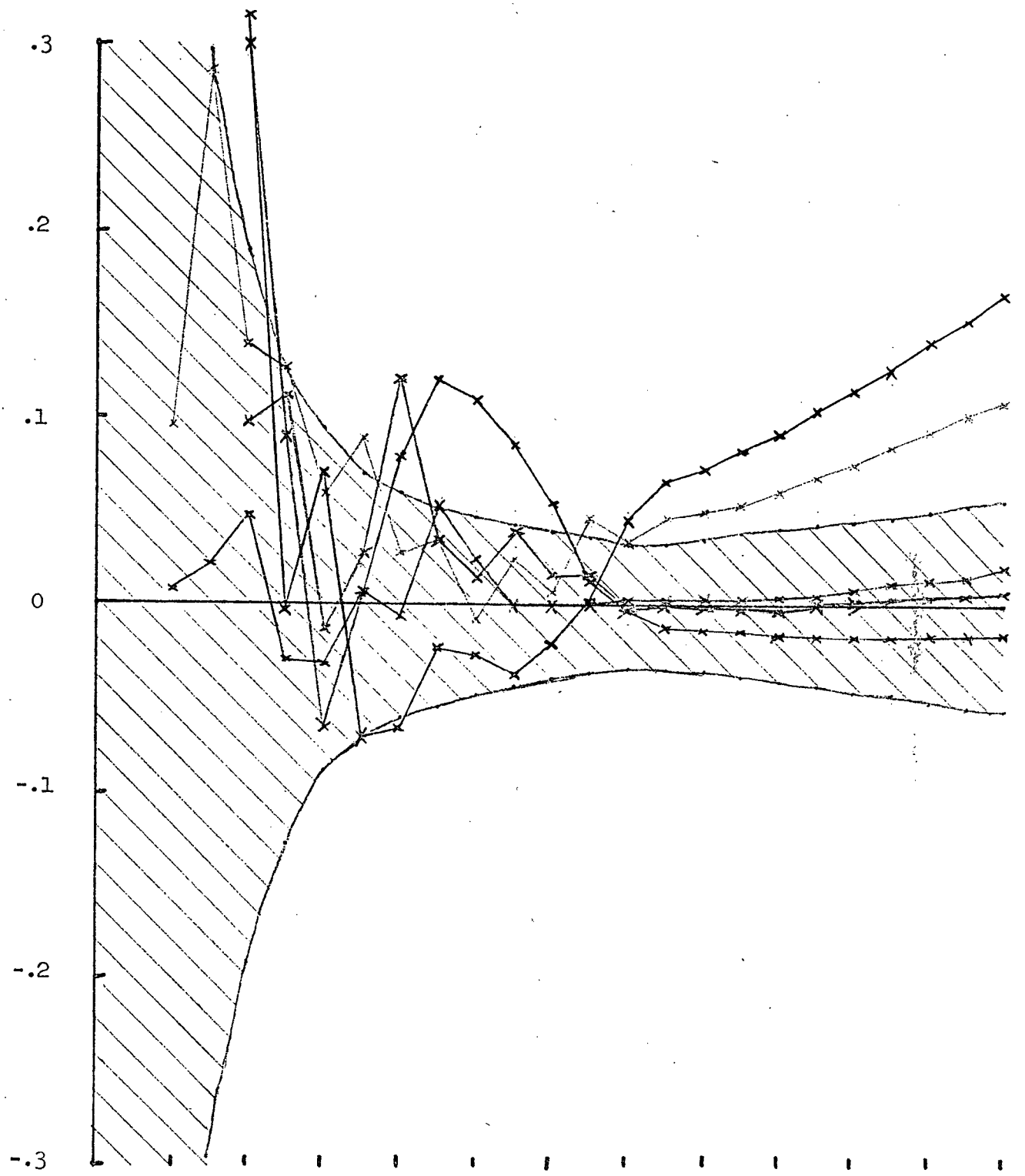

(f) $\dot{Z}$ Error, ft/sec

Figure 6 - (concl.)

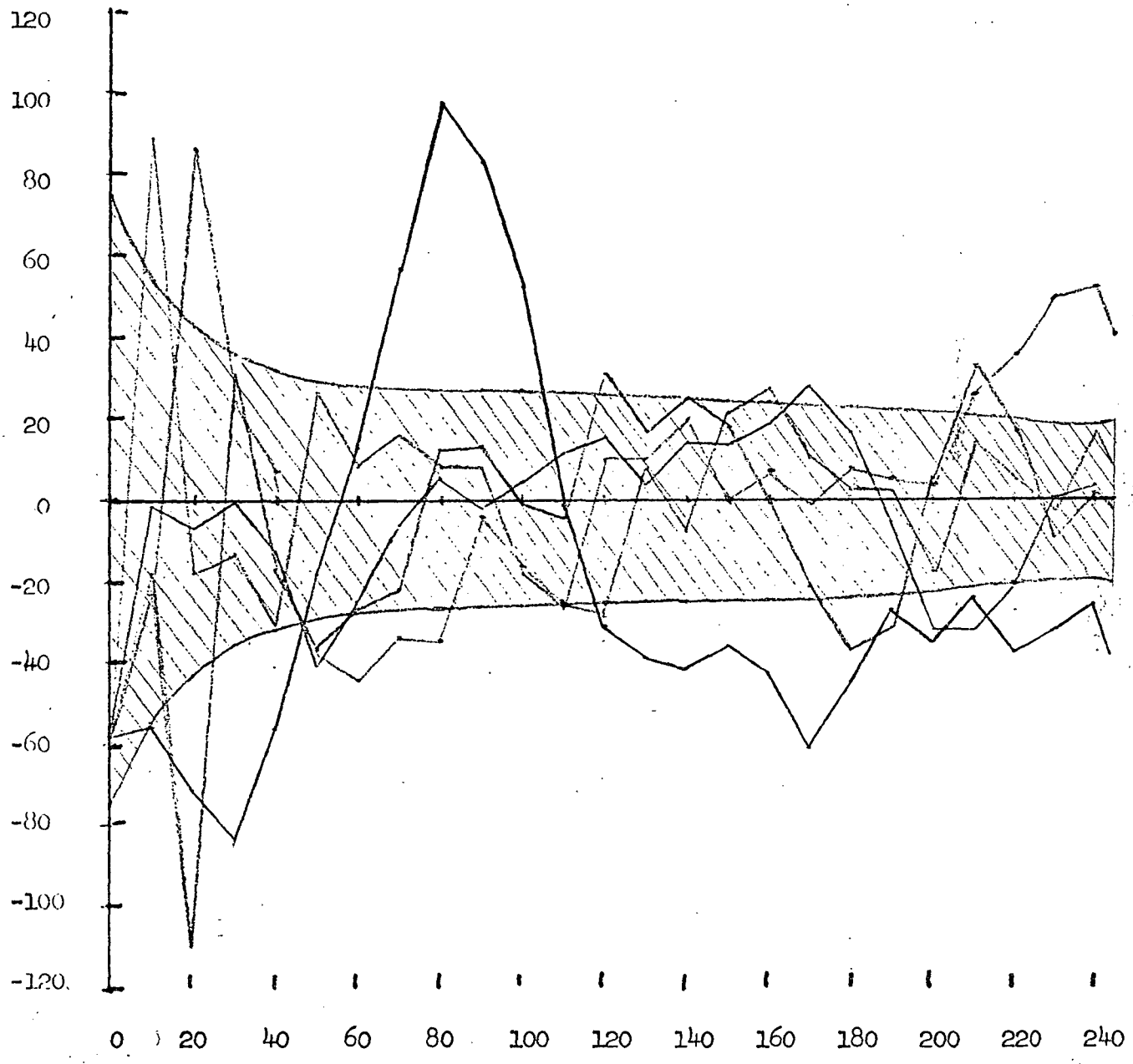

(a) X Error, ft

Figure 7 - Time History of Estimation Error With Microwave Scan Beam and Baro-Altimeter Data

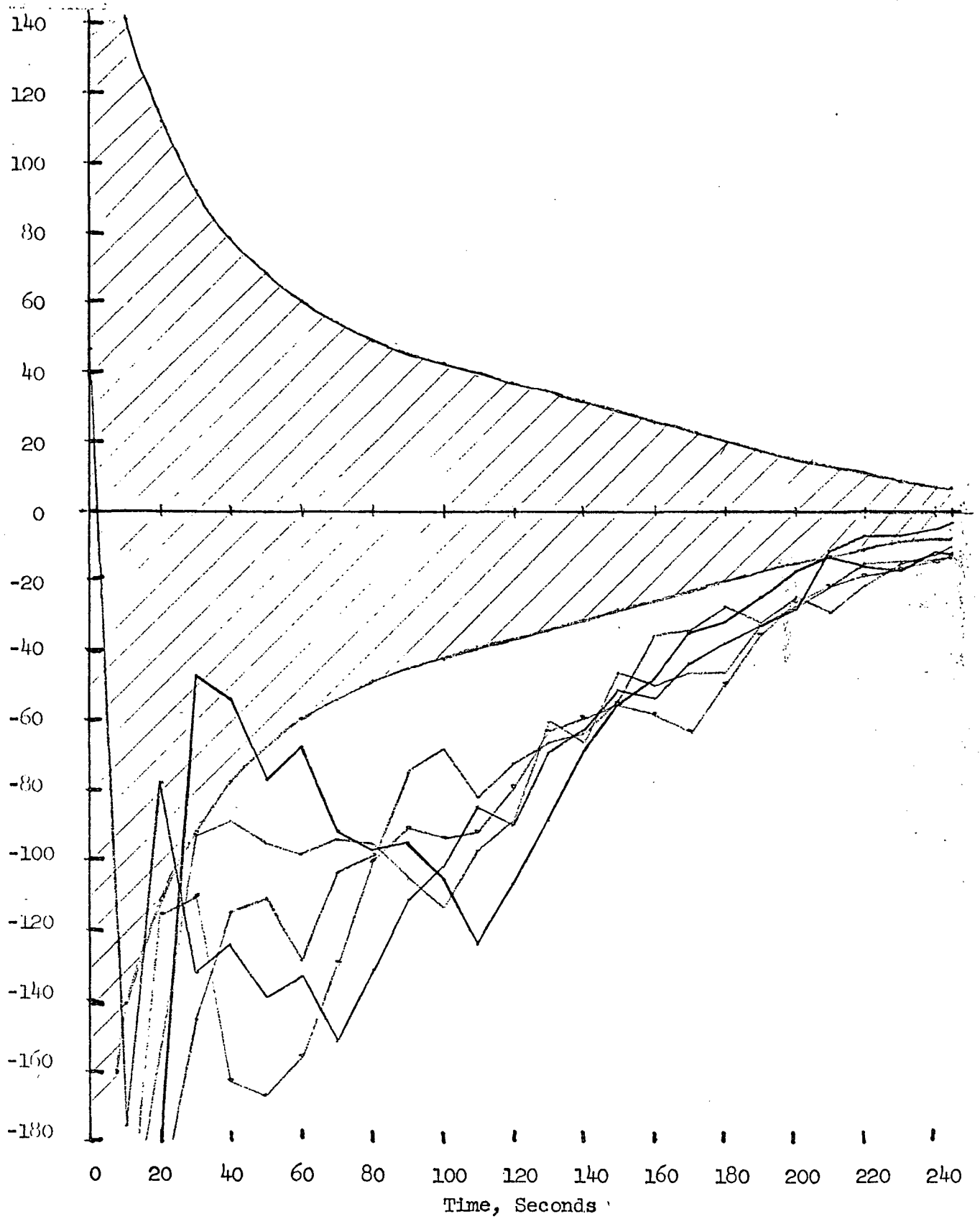

(b) Y Error, ft

Figure 7 - (cont'd)

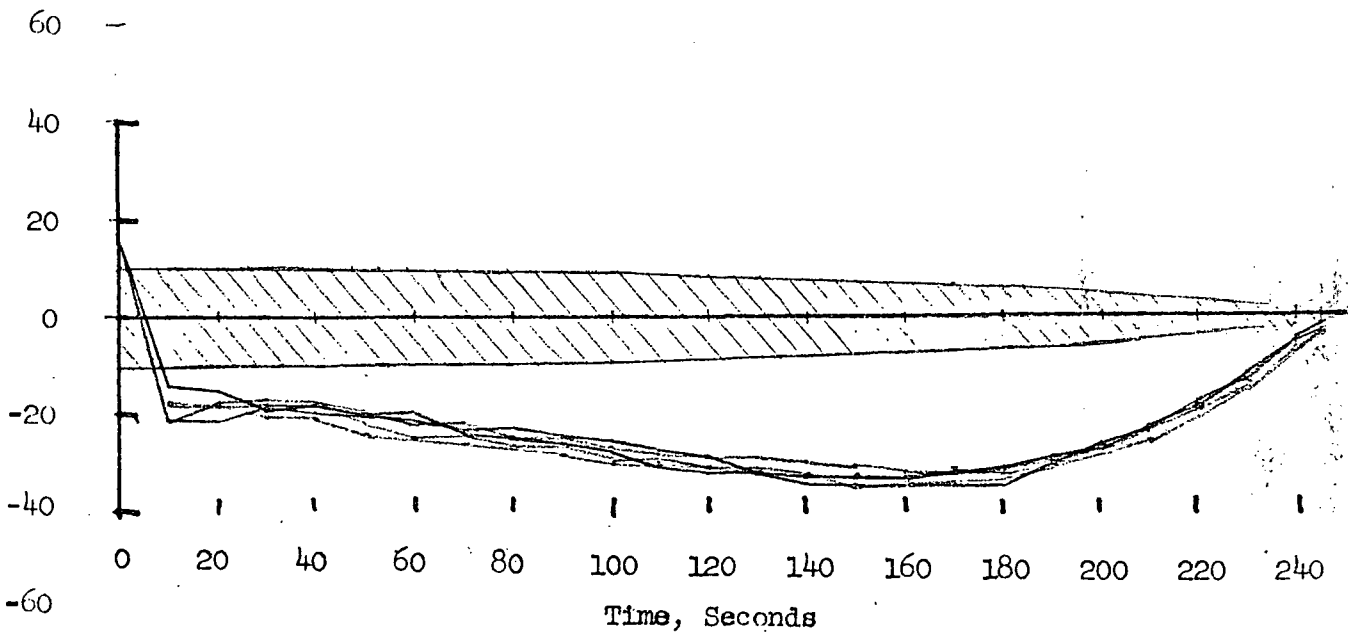

(c) Z Error, ft

Figure 7 - (cont'd)

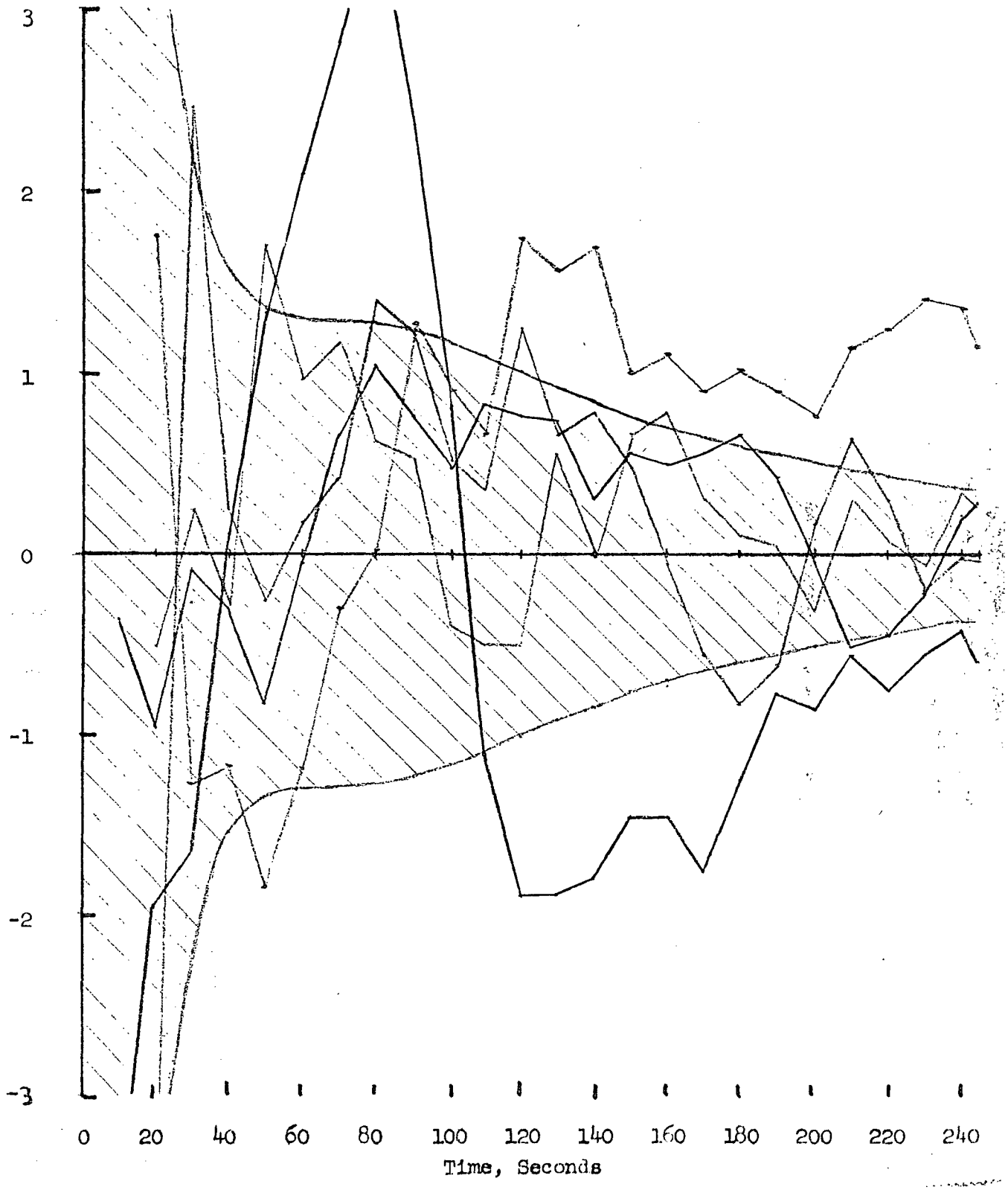

(d) $\dot{X}$ Error, ft/sec

Figure 7 - (cont'd)

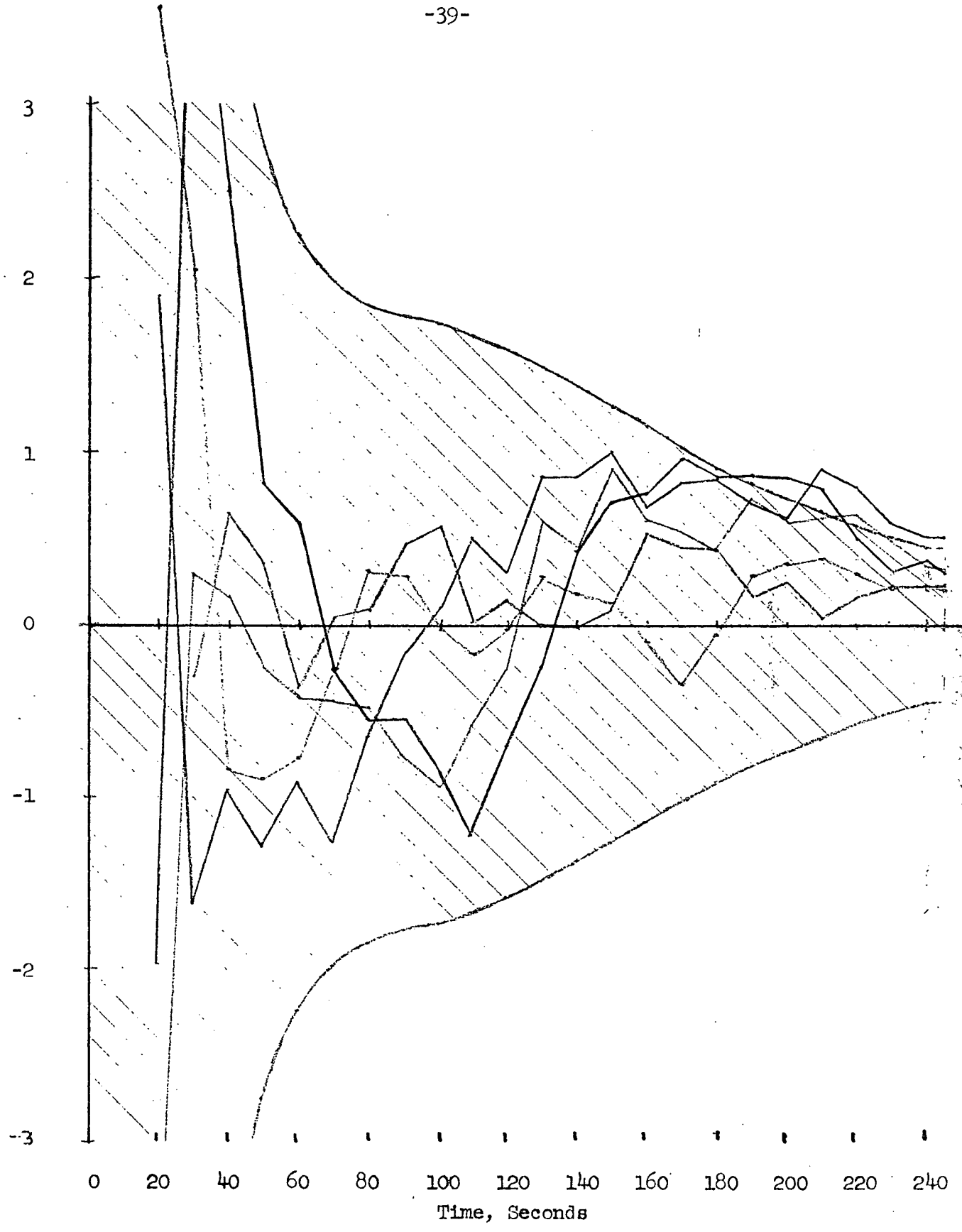

(e) $\dot{Y}$ Error, ft/sec

Figure 7 - (cont'd)

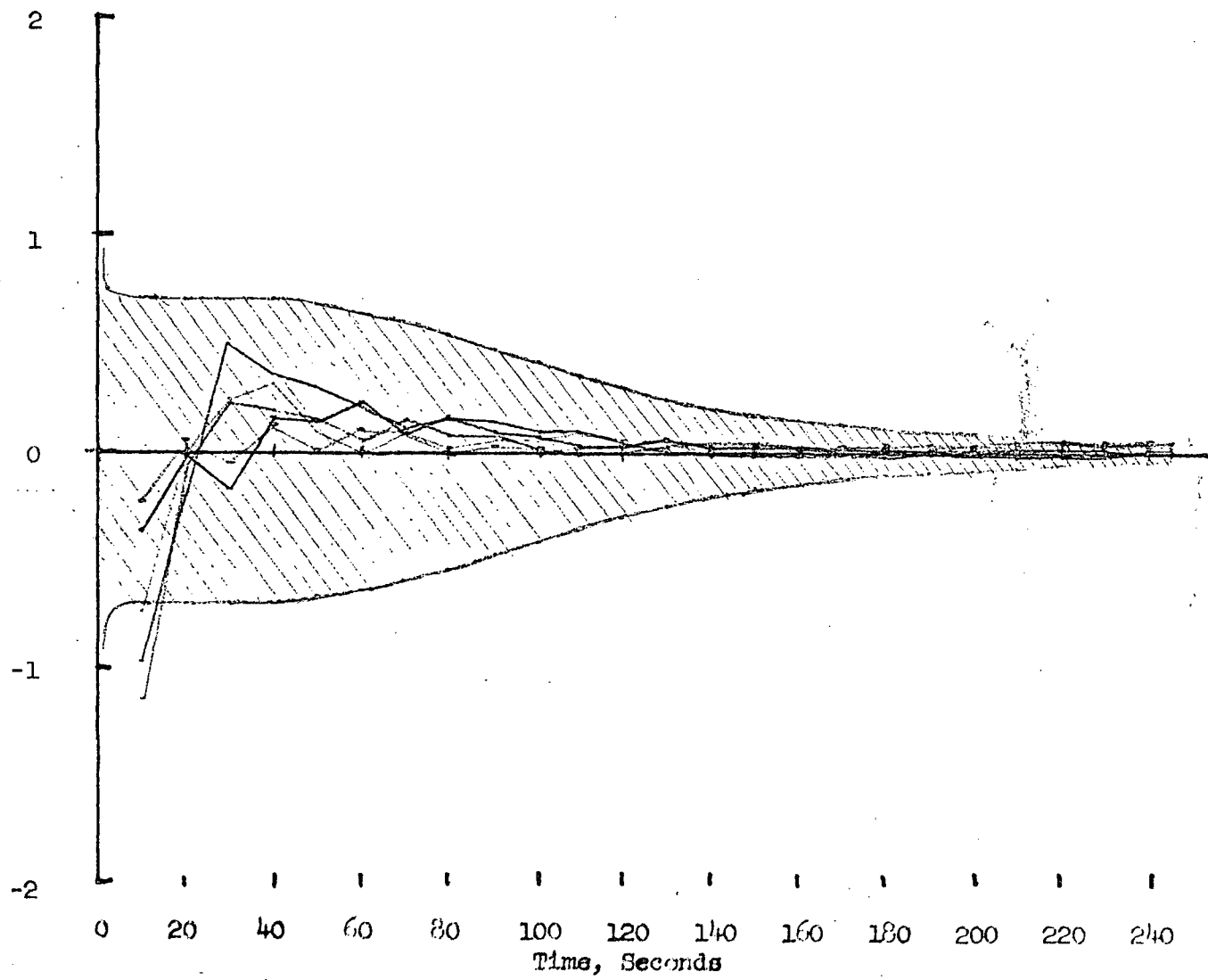

(f) $\dot{Z}$ Error, ft/sec

Figure 7 - (concl.)